

**Development and Comparison of Empirical Models for All-sky Downward
Longwave Radiation Estimation at the Ocean Surface Using Long-term
Observations**

**Jianghai Peng^{1,2,3,4}, Bo Jiang^{1,2*}, Hui Liang^{1,2}, Shaopeng Li^{1,2}, Jiakun Han^{1,2}, Thomas C.
Ingalls^{3,4}, Jie Cheng^{1,2}, Yunjun Yao^{1,2}, Kun Jia^{1,2}, and Xiaotong Zhang^{1,2}**

¹The State Key Laboratory of Remote Sensing Science, jointly sponsored by Beijing Normal University and
Institute of Remote Sensing and Digital Earth of Chinese Academy of Sciences, Beijing, China.

²China and Beijing Engineering Research Center for Global Land Remote Sensing Products, Institute of
Remote Sensing Science and Engineering, Faculty of Geographical Science, Beijing Normal University,
Beijing, China.

³Center for Global Discovery and Conservation Science, Arizona State University, Tempe, AZ, 85281, USA.

⁴School of Earth and Space Exploration, Arizona State University, Tempe, AZ, 85281, USA.

Corresponding author: Bo Jiang(bojiang@bnu.edu.cn)

Abstract

The ocean-surface downward longwave radiation (R_l) is one of the most fundamental components of the radiative energy balance, and it has a remarkable influence on air–sea interactions. Because of various shortcomings and limits, a lot of empirical models were established for ocean-surface R_l estimation for practical applications. In this paper, based on comprehensive measurements collected from 65 moored buoys distributed across global seas from 1988 to 2019, a new model for estimating the all-sky ocean-surface R_l at both hourly and daily scales was built. The ocean-surface R_l was formulated as a nonlinear function of the screen-level air temperature, relative humidity, cloud fraction, total column cloud liquid, and ice water. A comprehensive evaluation of this new model relative to eight existing models was conducted under clear-sky and all-sky conditions at daytime/nighttime hourly and daily scales. The validation results showed that the accuracy of the newly constructed model is superior to other models, yielding overall RMSE values of $\underline{13.44} \pm 4.82$ and $\underline{8.34} \pm 0.76$ W/m² under clear-sky conditions, and $\underline{15.64} \pm 9.5$ and 10.27 W/m² under all-sky conditions, at hourly and daily scales, respectively. Our analysis indicates that the effects of the total column cloud liquid and ice water on the ocean-surface R_l also need to be considered besides cloud cover. Overall, the newly developed model has strong potential to be widely used.

Keywords: Ocean surface, longwave radiation, empirical model, buoy

1 Introduction

The downward longwave radiation (R_l) at the ocean surface is the thermal infrared (4–100 μ m) radiative flux emitted by the entire atmospheric column over the ocean surface (Yu et al., 2018). The ocean-surface R_l is among the most important components of the heat flux across the ocean–atmosphere interface, which, in turn, shapes the climate state of both the atmosphere and ocean (Caniaux, 2005; Fasullo et al., 2009; Fung et al., 1984). Therefore, an accurate estimate of the ocean-surface R_l is crucial for studies of air–sea interactions and the climate and oceanic systems.

Although the ocean-surface R_l is ~~routinely~~ measured at most buoy sites, the available ocean-surface R_l measurements can not meet the needs of various applications because of the small number of buoys currently employed (especially moored buoys) and their sparse distribution across global oceans. Another way to get the R_l at the ocean surface is by using satellite-based or model reanalysis products. The ocean-surface R_l from satellite-derived products, such as the International Satellite Cloud Climatology Project (ISCCP) (Rossow & Zhang, 1995; Young et al., 2018) and Clouds and the Earth’s Radiant Energy System Synoptic Radiative Fluxes and Clouds (CERES/SYN1deg) (Doelling et al., 2013; Rutan et al., 2015) is usually generated using these satellite data and a radiative transfer model, which simulates the radiative transfer interactions of light absorption, scattering, and emission through the atmosphere with the input of given atmospheric parameters. However, radiative transfer models are not widely used in practice because of their ~~complexity~~ ~~complexity~~ and the difficulties associated with collecting all essential inputs. The ocean-surface R_l provided in model reanalysis products, such as the fifth generation of the European Centre for Medium-Range Weather Forecasts atmospheric reanalysis of the global climate (ERA5) (Hersbach et al., 2020) and the Modern-Era Retrospective analysis for Research and Applications, Version 2 (MERRA2) (Gelaro et al., 2017), is produced by assimilating various observations into an atmospheric model to get

the optimal estimates of the state of the atmosphere and the surface (Gelaro et al., 2017). Previous studies indicated that R_1 estimates from satellite-based products are generally in better agreement with buoy measurements than those obtained from reanalysis products (Pinker et al., 2014; Pinker et al., 2018; Thandlam & Rahaman, 2019). However, applications of the ocean-surface R_1 from these two kinds of products are limited due to their coarse spatial resolutions (most of them are coarser than 1°), limited periods (especially satellite-based products), and discrepancies in accuracy and consistency (Cronin et al., 2019). Hence, many parameterization and empirical models for estimating ocean-surface R_1 that can easily be implemented in practical use have been established during the past few decades (Bignami et al., 1995; Josey, 2003; Zapadka et al., 2001). Most of the commonly used R_1 estimation models were established using the relationship between R_1 and the relevant meteorological variables (i.e., air temperature, humidity, column integrated water vapor (IWV), and cloud parameters) or oceanic parameters (i.e., bulk sea surface temperature), which are usually obtained from in situ measurements or model simulations (Li & Coimbra, 2019; Li et al., 2017; Paul, 2021). It is known that most R_1 estimation models were originally developed for the land surface and were applied to the ocean surface directly without any alterations by assuming the atmospheric conditions are nearly the same over ocean and land surfaces (Bignami et al., 1995; Clark et al., 1974; Frouin et al., 1988; Josey, 2003). However, this assumption increases the uncertainty in R_1 estimates because of the significantly different water vapor profiles over ocean and land surfaces (Bignami et al., 1995). A few models built specifically for R_1 estimation at the ocean surface (Bignami et al., 1995; Josey, 2003; Zapadka et al., 2001) were usually developed using limited observations collected from buoy sites or cruise ships distributed within a specific region; hence, the robustness of these models were in doubt when applied globally. For example, Josey (2003) proposed a model for R_1 estimation at mid-~~to~~-high latitude seas with a satisfactory validation accuracy, but this new model performed worse over tropical seas with a tendency to underestimate R_1 by up to $10\text{--}15\text{ W/m}^2$. Moreover, most of the existing R_1 estimation models only work under clear-sky conditions, which are especially rare over ocean surfaces. Furthermore, most of these models only derive R_1 at instantaneous scales, yet the R_1 at the daily scale is more preferred across a range of applications. Therefore, a new, easily implemented model that can derive accurate and robust R_1 estimates at the global ocean surface under all-sky conditions at various temporal scales (e.g., instantaneous and daily) is required. More details about the existing R_1 estimation models are given in Section 2.

In addition, according to W Wang and Liang (2009b), the uncertainty of the ocean-surface R_1 estimation should be less than 10 W/m^2 for climate diagnostic studies. However, the performances of the most commonly used R_1 estimation models at the global ocean surface were not thoroughly evaluated in previous studies because of the few available in situ measurements. Fortunately, being aware of the significance of the energy budget in air-sea interactions (Centurioni et al., 2019), more and more platforms for radiative measuring have been built across global ocean surfaces during the past decades, so relatively comprehensive ocean-surface R_1 measurements can be collected today, which provide a good opportunity for modeling and comprehensive evaluations.

Overall, the main goal of this research is to establish a new empirical model for calculating the all-sky ocean-surface R_1 at instantaneous and daily scales based on globally distributed moored buoy measurements and other ancillary information. A comprehensive evaluation is conducted on the newly developed model relative to eight commonly used models for ocean-surface R_1 estimation under clear- and all-sky conditions at hourly and daily scales.

The organization of this paper is as follows. A review of the eight commonly used R_l estimation models is presented in Section 2. Section 3 introduces the data sets used in this research and the methods, including the new model development and model evaluation. Section 4 shows the results of the model validation, comparison, and analysis. The key conclusions and discussions are provided in Section 5.

2 Review of Previous Models

Many models were proposed for R_l calculation under various sky conditions at different temporal scales in previous studies. In this study, eight widely used models were selected for evaluation and Table 1 shows their basic information. According to the sky conditions under which these models could be used, the eight R_l estimation models were divided into two classes: R_l models under clear-sky conditions and under all-sky conditions, respectively. Details of the eight models are provided one by one in the following section. Note that the downward direction is defined as positive in this study.

Table 1

Eight Existing Models for Ocean-surface R_l Estimation, with Variables Explained in Table 2.

Sky Condition	Model	Abbr	Designed temporal scale	Reference
Clear-sky	$R_l = a\sigma T_a^4(1+b\sqrt{e})$	Mod1	Monthly	Brunt (1932)
	$R_l = \sigma T_a^4 \{1 - a \exp(-b(273 - T_a)^2)\}$	Mod2	5–15 minute	Idso and Jackson (1969)
	$R_l = a\sigma T_a^4 (e/T_a)^{1/7}$	Mod3	Instantaneous	Brutsaert (1975)
	$R_l = a\sigma T_a^4 [1 - \exp(-e^{T_a/2016})]$	Mod4	Daily	Satterlund (1979)
	$R_l = \sigma T_a^4 \left[1 - (1 + \epsilon) \exp\left\{ -\left(1.2 + 3\epsilon \right)^{1/2} \right\} \right]$ $\epsilon = 46.5 \left(\frac{e}{T_a} \right)$	Mod5	Instantaneous	Prata (1996)
All-sky	$R_l = \frac{\epsilon \sigma T_s^4 - \epsilon \sigma T_s^4 (a + b\sqrt{e}) (1 - \lambda C^2) + 4\epsilon \sigma T_s^3 (T_s - T_a)}{1 - \alpha_l}$	Mod6	Daily	Clark et al. (1974)
	$R_l = \sigma T_a^4 (a + be)(1 + dC^2)$	Mod7	Hourly	Bignami et al. (1995)
	$R_l = \sigma \{T_a + aC^2 + bC - d + g(D + f)\}^4$	Mod8	Hourly	Josey (2003)

2.1 Under clear-sky condition

Among the eight models, there are five R_l estimation models that could only be used under clear-sky conditions.

Brunt (1932) developed the first R_l estimation model (named Mod1) for land surfaces, which relates the monthly mean R_l to the screen-level water vapor and air temperature, as Equation (1) shows:

$$R_l = a_1 \sigma T_a^4 (1 + b_1 \sqrt{e}) \quad (1)$$

where a_1 and b_1 are empirical coefficients, T_a is the monthly mean screen-level air

temperature (K), e is the monthly mean screen-level water vapor pressure (mbar), and σ is the Stefan–Boltzmann constant, defined as $5.67 \times 10^{-8} \text{ W}/(\text{m}^2 \cdot \text{K}^4)$. In the study of Brunt (1932), the two coefficients a_1 and b_1 were suggested as 0.52 and 0.125 based on observations collected from Benson, South Oxfordshire, England. The validation results of Mod1 showed a correlation coefficient as high as 0.97 based on the collected samples. However, Swinbank (1963) pointed out that the validation results of Mod1 for other regions where variations in the humidity and T_a were different from those in Benson were worse. Despite these limitations, as the first empirical R_1 estimation model in a simple format, Mod1 has been widely used to construct the coupling between hydrological and atmospheric models (Habets et al., 1999; Lohmann et al., 1998).

Different from Mod1, the model developed by Idso and Jackson (1969) (named Mod2) was based on the theoretical consideration that the effective emittance of an atmosphere is solely temperature-dependent; hence, the screen-level T_a is the only input of Mod2 for calculating R_1 :

$$R_1 = \sigma T_a^4 \{1 - a_2 \exp(-b_2(273 - T_a)^2)\} \quad (2)$$

where a_2 and b_2 are empirical coefficients, which were defined as 0.261 and 7.770×10^{-4} , respectively, by Idso and Jackson (1969) based on experimental data at four sites located in Arizona, Alaska, Australia, and the Indian Ocean, obtained at intervals of 5 to 15 minutes. Idso and Jackson (1969) thought that Mod2 might be efficient at all latitudes for different seasons, as it has been developed by using observations from diverse locations. Since publication, Mod2 has been employed in relevant researches like evaporation estimation (Cleugh et al., 2007; Vertessy et al., 1993) and ocean-ice modeling (Saucier et al., 2003).

Afterwards, Brutsaert (1975) proposed a simple model for computing R_1 by directly solving the Schwarzschild's transfer equation (Schwarzschild, 1914) under clear skies and standard atmospheric conditions (i.e., the U.S. 1962 standard atmosphere). This model is denoted as Mod3, and is described as follows:

$$R_1 = a_3 \sigma T_a^4 (e/T_a)^{1/7} \quad (3)$$

where a_3 is defined as a constant equal to 1.24, as determined during the Schwarzschild's transfer equation solving process. Explicit physical theory is reflected in Mod3. The term $(e/T_a)^{1/7}$, regarded as the atmospheric emissivity, tends to zero when the water vapor content is very little. However, Prata (1996) indicated that the atmospheric emissivity tends to a certain constant value even without water vapor, such as values from 0.17 to 0.19 when only CO_2 is present (Staley & Jurica, 1972). The estimates from Mod3 are usually used as the necessary inputs of hydrological models (Pauwels et al., 2007; Rigon et al., 2006) and climate models (Mills, 1997).

Aase and Idso (1978) found that Mod2 and Mod3 performed poor when T_a was below freezing. To address this issue, Satterlund (1979) proposed a model (named Mod4) to compute R_1 by reformatting T_a and e , as follows:

$$R_1 = a_4 \sigma T_a^4 [1 - \exp(-e^{T_a/2016})] \quad (4)$$

where a_4 is an empirical coefficient and defined as 1.08 by Satterlund (1979) based on collected daily R_1 measurements at one site in Sidney, Montana, USA. After validation and comparison, Satterlund (1979) concluded that Mod4 outperformed Mod2 and Mod3 under extreme conditions in terms of temperature and humidity and performed comparably with the two models for other cases. As such, the R_1 estimates from Mod4 have been used in studies such

as snow pack evolution (Douville et al., 1995) and hydrological models (Schlosser et al., 1997). However, because the model does not contain a constant term, the application of Mod4 should be done with caution if the surface water vapor pressure is very close to zero.

With the development of radiation measuring instruments and technology, several new R_l estimation models have been proposed, such as the model proposed by Prata (1996) (named Mod5), as follows:

$$R_l = \sigma T_a^4 \left[1 - (1 + 46.5 \left(\frac{e}{T_a} \right)) \exp \left\{ - \left(a_5 + 46.5 b_5 \left(\frac{e}{T_a} \right) \right)^{1/2} \right\} \right] \quad (5)$$

where a_5 and b_5 are empirical coefficients, defined as 1.2 and 3.0 in the study of Prata (1996) and Robinson (1947; 1950). As with Mod1–Mod4, Mod5 is also dependent on T_a and e but contains a majorly revised right term (in the square brackets), which is regarded as the emissivity. After extensive validation and comparison, Prata (1996) claimed Mod5 outperformed or performed similar to other R_l estimation models, including Mod1–Mod4, in areas within the polar region, mid-latitudes, and tropical regions. Hence, Mod5 has been applied widely, from studies of snowmelt modeling (Jost et al., 2009) to urban energy budget (Nice et al., 2018; Oleson et al., 2008).

To sum up, all five R_l estimation models (Mod1–Mod5) that only work under clear-sky conditions take T_a and/or e as inputs. Such an approach is in agreement with the research of Kjaersgaard et al. (2007) who found that R_l is mainly emanated from the low-level atmosphere that can be adequately characterized in terms of T_a and humidity under clear-sky conditions (Diak et al., 2000; Ellingson, 1995; Prata, 1996). Moreover, the five models were all established by using measurements from different regions at various timescales, and they can be employed at any timescale (see Table 1) regardless of the temporal resolution of the original measurements used for modeling.

2.2 Under all-sky condition

Three R_l estimation models that can work under all-sky conditions were evaluated in this paper. Comparing to the above five models, ancillary information (e.g., clouds) should be taken into account in addition to T_a and e in the three models, and the three models were developed specifically for ocean surfaces.

Based on the model developed by Clark et al. (1974) for the all-sky net longwave radiation at the ocean surface ($R_{l,net}$, the difference between the downward and upward longwave radiation) calculation, Josey (2003) proposed a revised model (named Mod6) to estimate the all-sky ocean-surface R_l by getting rid of the ocean-surface upward longwave radiation as:

$$R_l = \frac{\varepsilon_s \sigma SST^4 - \varepsilon_s \sigma SST^4 (a_6 + b_6 \sqrt{C}) (1 - \lambda C^2) - 4 \varepsilon_s \sigma SST^3 (SST - T_a)}{1 - \alpha_s} \quad (6)$$

where ε_s is the sea surface emissivity, defined as a constant value of 0.98, and SST is the sea surface temperature (K); hence, the term $\varepsilon_s \sigma SST^4$ is the upward longwave radiation at the ocean surface. α_s is the sea surface longwave radiation reflectivity, defined as a constant value of 0.045, C is the cloud cover (0–1; dimensionless), λ is a latitude-dependent coefficient that represents the cloud amount, and a_6 and b_6 are empirical coefficients. Based on measurements (i.e., R_l , T_s , and C) collected from the Chemical and Hydrographic Atlantic Ocean Section (CHAOS) in the northeast Atlantic in 1998, a_6 and b_6 were determined as 0.39 and -0.05 (Clark et

al., 1974; Josey, 2003), and λ at a given latitude can be taken from Josey et al. (1997). Josey (2003) validated Mod6 and the results showed that Mod6 tended to overestimate the instantaneous R_i measurements from CHAOS by 11.70 W/m². The estimates from Mod6 have been applied in hydrodynamic models (Grayek et al., 2011) and atmospheric boundary layer models (Deremble et al., 2013).

Based on hourly cruise measurements (i.e., R_i , T_a , and C) collected in the Mediterranean Sea during the period from 1989 to 1992, Bignami et al. (1995) proposed an empirical model to calculate the ocean-surface all-sky R_i (named Mod7) as follows:

$$R_i = \sigma T_a^4 (a_7 + b_7 e)(1 + c_7 C^2) \quad (7)$$

where a_7 , b_7 , and c_7 are empirical coefficients defined as 0.684, 0.0056, and 0.1762, respectively. Bignami et al. (1995) presented validated RMSE values for Mod7 which ranged from ~14 W/m² at the hourly scale to ~9 W/m² at the daily scale. Mod7 has been utilized by the Mediterranean Forecasting System for predictions of currents and biochemical parameters (Pinardi et al., 2003), coupled ocean–atmosphere climate models (Dubois et al., 2012) as well as generation of the Atlantic Ocean heat flux climatology (Lindau, 2012).

Also based on the measurements collected from CHAOS, Josey (2003) assessed the accuracy of Mod7 and found that this model tended to underestimate the all-sky R_i by 12.10 W/m² at the instantaneous scale. After analyzing the shortcomings of Mod6 and Mod7, Josey (2003) proposed a new model (named Mod8) for all-sky ocean-surface R_i calculation through a revision of T_a by using the same samples:

$$R_i = \sigma \{T_a + a_8 C^2 + b_8 C - c_8 + d_1 (D + e_1)\}^4 \quad (8)$$

where a_8 , b_8 , c_8 , d_1 , and e_1 are empirical coefficients determined as 10.77, 2.34, 18.44, 0.84, and 4.01, respectively, D is the dew point depression, and T_a is the temperature (K) (see Equation (11)). Estimates of R_i obtained with Mod8 agreed to within 2 W/m² in the mean bias of 10 minute measurements at middle-high latitudes. The estimates from Mod8 have been used as essential input in simulations of ocean–atmosphere interactions in the Arctic shelf (Cottier et al., 2007).

Overall, it was thought that variations in the all-sky ocean-surface R_i were related to T_a , e , and cloud information (e.g., cloud cover and cloud amount) in previous studies. However, Fung et al. (1984) pointed out that other relevant cloud information, such as the cloud base height (CBH) and cloud optical thickness, also have a significant influence on ocean-surface longwave radiation. Therefore, more efforts should be made to increase the R_i estimation accuracy under all-sky conditions.

3 Data and Methodology

In order to develop a new all-sky ocean-surface R_i estimation model, the meteorological and radiative observations from 65 moored buoys and the cloud parameters from the ERA5 reanalysis product from 1988 to 2019 were applied. Afterwards, the newly developed model and the eight commonly used models (Mod1–Mod8) were evaluated against the moored R_i measurements under clear- and all-sky conditions at hourly/daily scales

3.1 Data and pre-processing

Table 2 lists all the variables employed in this paper and their information. The instantaneous timescale can be defined as timescales ranging from a 3 minute average to hourly average (Bignami et al. (1995); K Wang and Liang (2009a); hence, two timescales, hourly and daily, were considered in this study for model evaluation as in previous studies (Bilbao & de Miguel, 2007; Kjaersgaard et al., 2007; Sridhar & Elliott, 2002). Note that Mod1 was also used at the two timescales (Guo et al., 2019) though it was originally established with monthly samples. More details about the data are given below.

Table 2

Variables: Explanations and Sources

Abbreviation	Full name	Time scales	Unit	Source
RH	Relative humidity	Daily/hourly	%	In situ
e	Water vapor	Daily/hourly	hPa	Calculated
T _a	2-m air temperature	Daily/hourly	K	In situ
T _s	Sea surface temperature	Daily/hourly	K	In situ
D	Dew point depression	Daily/hourly	K	Calculated
CI	Clearness index	Daily/hourly	0-1	Calculated
C	Fractional cloud cover	Daily/hourly	0-1	Calculated
clw	Total column cloud liquid water	Daily/hourly	g/m ²	ERA5
ciw	Total column cloud ice water	Daily/hourly	g/m ²	ERA5
R _l	<u>Downward longwave radiation</u>	<u>Daily/hourly</u>	<u>W/m²</u>	<u>In situ</u>
R _g	<u>Downward shortwave radiation</u>	<u>Daily/hourly</u>	<u>W/m²</u>	<u>In situ</u>
DSR _{toa}	<u>Extraterrestrial solar radiation (DSR_{toa})</u>	<u>Daily/hourly</u>	<u>W/m²</u>	<u>Modeled</u>

3.1.1 Measurements from moored buoys

All measurements were collected from 65 moored buoy sites, whose latitudes range from 47°S to 59.5°N, as shown in Figure 1. The majority of moored buoy sites were located in tropical seas (23.5°S–23.5°N), and relatively few buoys were in the high-latitude seas of the Northern Hemisphere (>50°N) and the mid-high latitude seas of the Southern Hemisphere (>30°S).

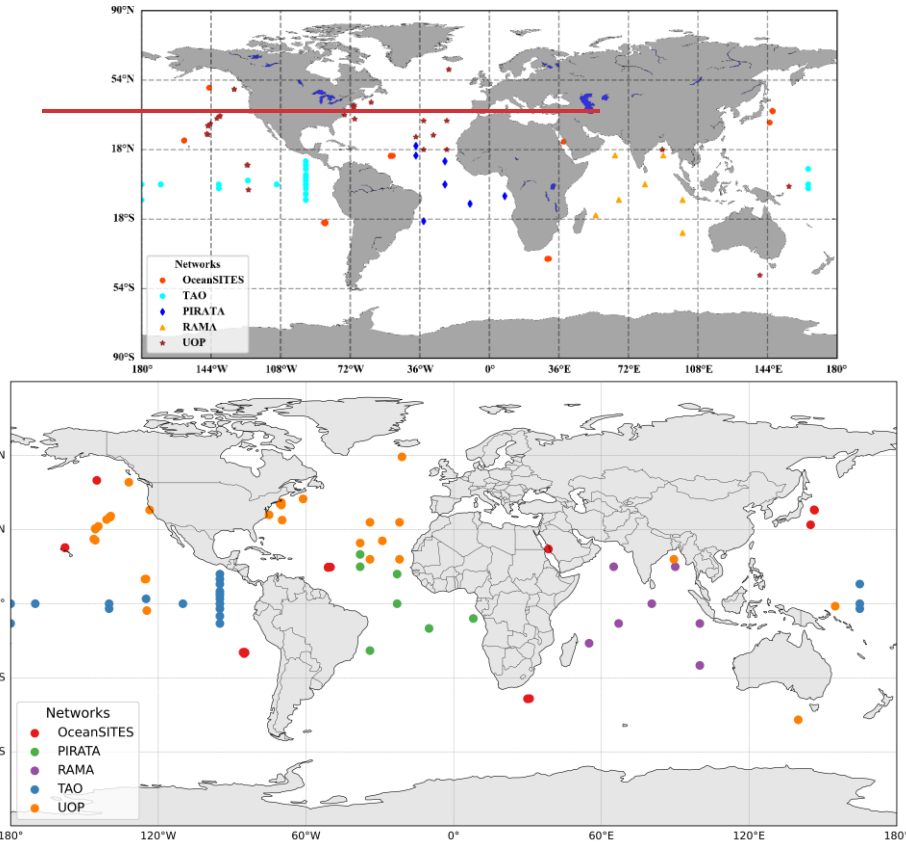


Figure 1. Spatial distribution of the 65 moored buoys.

The moored buoy sites in this study belong to five well-known observation network/programs, including the Upper Ocean Processes Group (UOP), Tropical Atmosphere Ocean/Triangle Trans-Ocean Buoy Network (TAO/TRITON), Pilot Research Moored Array in the Tropical Atlantic (PIRATA), Research Moored Array for African–Asian–Australian Monsoon Analysis and Prediction (RAMA), and OceanSITES. Launched by the Woods Hole Oceanographic Institution (WHOI), UOP mainly focuses on studying the physical processes of the air-sea interface and the epipelagic, and its buoys are equipped with oceanographic and meteorological sensors. The UOP measurements accurately quantify annual cycles of wind stress and net air-sea heat exchange in the Southern Ocean (Schulz et al., 2012). Twenty-two sites form the UOP, and data from all were used in this study. TAO/TRITON (McPhaden et al., 1998) in the tropical Pacific, PIRATA (Bourlès et al., 2008) in the tropical Atlantic, and RAMA in the tropical Indian Ocean (McPhaden et al., 2009) are all part of the Global Tropical Moored Buoy Array (GT MBA) program (McPhaden et al., 2010). Extensive quality control was done by GT MBA prior to dissemination of the data (Freitag, 1999; 2001; Lake, 2003; Medovaya et al., 2002), and

they have been used for monitoring, understanding, and forecasting the El Niño–Southern Oscillation (ENSO) and monsoon variability (McPhaden et al., 2009). Data from 35 GTMBA sites (TAO, 21; PIRATA, 7; RAMA, 7) were used in this study. The OceanSITES network is composed of buoys funded by oceanographic researchers across the globe. The goal of the OceanSITES program is to facilitate the use of high-quality multidisciplinary data from fixed sites in the open ocean (Cronin et al., 2019). Eight sites from OceanSITES were utilized, specifically: OS_PAPA, OS_KAUST, OS_NTAS, OS_KEO, OS_ARC, OS_JKEO, OS_STRATUS, and OS_WHOTS. In this study, the routine measurements made at moored buoys, including radiative measurements (e.g., ocean-surface downward shortwave radiation R_g) and meteorological measurements (e.g., T_a and RH) were collected and used; other variables (e.g., e , D , and CI) were calculated from these measurements. More information regarding these data sets is found in Table 3.

Table 3

Descriptions of Different Networks

Network/Program	No. of sites	Period	Observation frequency	Variables	URL
UOP	22	1988-2017	1 hour	R_i , R_g , T_a , RH	http://uop.whoi.edu/index.html
TAO/TRITON	21	2000-2019	10 min	R_i , R_g , T_a , RH	https://www.pmel.noaa.gov/tao/drupal/disdel/
RAMA	7	2004-2019	10 min	R_i , R_g , T_a , RH	https://www.pmel.noaa.gov/tao/drupal/disdel/
PIRATA	7	2006-2019	10 min	R_i , R_g , T_a , RH	https://www.pmel.noaa.gov/tao/drupal/disdel/
OceanSITES	8	2000-2018	1 hour	R_i , R_g , T_a , RH	http://www.oceansites.org/

3.1.1.1 Radiative measurements

At each moored buoy, R_i is routinely measured by an Eppley Precision Infrared Radiometer (PIR) with a nominal accuracy of $\pm 1\%$ (Richard E. Payne & Anderson, 1999), and R_g is routinely measured by an Eppley Laboratory precision spectral pyranometer (PSP) with a calibration accuracy of $\pm 2\%$ (Freitag, 1994). The PIR and PSP are deployed approximately 3 m above sea level. All measurements are quality controlled by their providers. To ensure data quality, a two step approach was implemented; 1) only observations flagged as ‘high quality’ by the data providers were considered, and 2) data was manually inspected by the authors for any irregularities. Additionally, the R_i measurements above 450 W/m^2 were removed, as suggested by Josey (2003).

As pointed out by Pascal and Josey (2000), the main errors in measuring R_i are from the shortwave leakage and differential heating of the sensor. ~~Therefore, the These~~ errors (ΔR_i) in R_i observations ~~were can be~~ corrected according to Pascal and Josey (2000) ~~as~~:

$$\Delta R_i = (a + \lambda) R_g + b R_g^2 \quad (9)$$

where $a = 4.34 \times 10^{-3}$, $\lambda = 0.011$, and $b = 1.72 \times 10^{-6}$. ~~However, this correction was not applied in our study, as (a) differential heating corrections had already been performed by the data providers, and (b) the R_i spikes associated with sensor degradation were not present across all deployments, making a universal correction inappropriate. Hence, the R_i measurements at a sampling frequency less than one hour were first corrected. After that, selected We also~~

compared the results with and without the correction and found that the conclusions remained unchanged.

All R_i measurements whose sampling frequency was less than one hour were aggregated into hourly means as long as 80% of the measurements in one hour were available, and the hourly data were aggregated into daily means as long as 24 hourly data in one day were available.

Note that the errors of the measured R_g induced by buoy rocking motions, sensor tilting, and aerosol accumulation (Medovaya et al., 2002) were too small to be considered here. At last, total, 47,266 samples at the daily scale and 1,275,308 samples at the hourly scale during the period from 1988 to 2019 were used in this study. For better comparison, the hourly samples used for independent validation were further divided into daytime ($R_g > 120 \text{ W/m}^2$) and nighttime conditions ($R_g \leq 120 \text{ W/m}^2$), with 147,981 samples in daytime and 210,057 in nighttime.

3.1.1.2 Meteorological and oceanic variables

Two meteorological measurements, RH and T_a , were collected at the moored buoy sites. The instrument used for measuring RH and T_a is a Rotronic MP-100F, deployed about 3 m above the sea level. The instrument produced accuracies of 2.7% and 0.2 K (Lake, 2003) for RH and T_a , respectively, which are also too small to influence the accuracy of the R_i estimation. Similar to the radiative measurements, RH and T_a were both strictly screened and then aggregated into hourly and daily means.

On the contrary, On the other hand, the sea surface temperature (SST) was measured at about 1 m below the sea level using a high-accuracy conductivity and temperature recorder (SBE37/39; Sea Bird Electronics) with an accuracy of 0.002 K. According to Donlon et al. (2002), there is a strong correlation between body SST and skin SST. Although wind speed has a significant effect on this relationship, a constant correction offset can be applied when the wind speed exceeds 6 m/s (Alappattu et al., 2017). In fact, 83% of the samples had wind speeds above 4 m/s, and as suggested by Vanhellemont (2020), the bulk SST measured at moored buoys can be adjusted to the skin SST by using a correction offset of 0.17 K.

3.1.1.3 Calculation of other variables

Three variables, including e , D , and CI , were calculated with the RH, T_a , and R_g , measurements separately. Therefore, these three variables at hourly and daily scales were obtained from the corresponding measurements. Specifically, the daily (hourly) mean e was calculated from the daily (hourly) RH using the following equation:

$$e = 6.1121 \frac{RH}{100} \exp\left(\frac{17.502T_a}{T_a + 240.97}\right) \quad (10)$$

Note that Equation (10) only works when T_a is in the range -30–50 °C (Buck, 1981), and T_a should be in items of °C.

The daily (hourly) dew point depression D was calculated according to Josey (2003) and Henderson-Sellers (1984) as:

$$D = 34.07 + 4157 / \ln(2.1718 * 10^8 / e) - T_a \quad (11)$$

The clearness index (CI) is calculated as the ratio of the surface R_g to the extraterrestrial

solar radiation (DSR_{toa}) (Ogunjobi & Kim, 2004). CI generally represents the atmospheric transmissivity affected by permanent gases, aerosols, and the optical thickness of the clouds (Alados et al., 2012; Flerchinger et al., 2009; Gubler et al., 2012; Jiang et al., 2015; Meyers & Dale, 1983), and it is widely used in radiation related researches (Iziomon et al., 2003; Jiang et al., 2016; Jiang et al., 2015; Richard E Payne, 1972). The value of CI is between 0 and 1, where a larger CI value represents a clearer sky. The hourly CI can be calculated as follows:

$$CI = \frac{R_g}{DSR_{toa}} \quad (12)$$

However, during nighttime, the hourly CI cannot be calculated by Equation (12) directly because of a lack of R_g values; hence, it was calculated based on a 24-hour solar radiation window centered on the hourly observation as suggested by Flerchinger et al. (2009). The daily CI was calculated as the average of all hourly CI values in a day for the sake of considering atmosphere variations at nighttime.

In this paper, CI was utilized to determine the condition as clear-sky when its value was greater than 0.7 at both hourly and daily scales. Additionally, it was found that the cloud cover derived from CI would help to improve the model performance after multiple experiments, especially at nighttime. Therefore, CI was also used to calculate the cloud cover. Specifically, the cloud fraction was linearly interpolated between $C = 1.0$ at a CI value of 0.4 for complete cloud cover to $C = 0.0$ at a CI value of 0.7 for cloudless, both at daily and hourly scales according to Flerchinger et al. (2009). Because of the different calculation of CI during daytime and nighttime, the uncertainty in the calculated cloud cover was different; hence, the R_i estimates at the hourly scale were further examined at daytime and nighttime. Therefore, all meteorological factors (RH , T_a , e , and D) at daily and at hourly scales were respectively prepared accordingly.

3.1.2 Cloud parameters from the ERA5 reanalysis data set

As described above, the cloud cover represented by the fraction (C) is usually taken into account when estimating R_i affected by clouds. However, in this study, two more cloud-related parameters, including clw and ciw (see Table 2+), from the ERA5 reanalysis product were also considered in the modeling. The total amount of liquid water per unit area in the air column from the base to the top of the cloud is called the total column cloud liquid water (clw), and its chilled counterpart (ice) is called the total column cloud ice water (ciw) (Nandan et al., 2022). ERA5 is the fifth generation atmospheric reanalysis product, and it was produced based on 4D-Var data assimilation using the Integrated Forecasting System (IFS) with an enhanced spatial resolution (0.25°) and time resolution (hourly) compared to its previous version ERA-interim (Hoffmann et al., 2019) from 1979 to present. Clouds in ERA5 are represented by a fully prognostic cloud scheme, in which cloud fractions and cloud condensates obey mass balance equations (Tiedtke, 1993). The ERA5 clw values are in good agreement with those obtained from radiosonde observations (Nandan et al., 2022). Overall, relative to ERA-interim, ERA5 shows reduced biases in the total ice water path versus other satellite-based observational products. Therefore, the two cloud parameters were extracted from the locations of the 65 moored buoy sites directly at the hourly scale, and then their daily means were calculated by averaging the 24 valid hourly values. ERA5 cloud product is available on the Climate Data Store (CDS) cloud server (<https://cds.climate.copernicus.eu/cdsapp#!/search?type=dataset>).

Overall, 70% of the samples at each moored buoy site, including 33,151 daily samples and 917,270 hourly samples, were randomly selected for new model training and calibration of

the eight previous models (Mod1– Mod8). The other 30% of the data at each site, including 14,115 daily samples and 358,038 hourly samples (daytime: 147,981; nighttime: 210,057), were used for model validation.

3.2. Methodology

A new model that could estimate ocean-surface R_i under all-sky conditions at both hourly and daily scales was developed based on the moored measurements and ERA5 cloud parameters. Moreover, the eight evaluated R_i models were all recalibrated so as to evaluate the model's accuracy objectively. Based on the corresponding validation samples, the R_i values produced by the nine models were compared under clear-sky and all-sky conditions at hourly and daily scales, where the comparison at the hourly scale was further divided into daytime and nighttime values.

3.2.1 New R_i estimation model development

As mentioned above, T_a and the humidity-related factors (e.g., RH) were enough to characterize the variations in R_i under clear-sky conditions. However, for cloudy skies, R_i is enhanced by the cloud base emitting (T Wang et al., 2020; Yang & Cheng, 2020). Cloud cover is one of the most commonly used cloud-related parameters. In addition, theoretically, the cloudy-sky R_i is significantly influenced by the cloud's base temperature, which is determined by the CBH; hence, CBH is thought to be necessary in determining R_i under cloudy-sky conditions (Viúdez-Mora et al., 2015). However, it is difficult to obtain the CBH accurately, especially for partly cloudy skies (Zhou & Cess, 2001) because of the unavailability of the cloud's geometrical thickness (Yang & Cheng, 2020). Therefore, other parameters that could provide information on the CBH were explored. In the study of Hack (1998), a physical correlation between clw and CBH was revealed for most cases, while clw was successfully used as an effective surrogate of the CBH in the study of Zhou and Cess (2001). However, Zhou et al. (2007) pointed out that the effects of ice clouds on R_i should also be considered when the atmospheric water vapor is low or at high latitudes, which means that ciw also needs to be taken into account. Inspired by these studies, clw and ciw, both in logarithmic form, were introduced in the development of a new model named Modnew, in which R_i under all-sky conditions at the ocean surface was related to five parameters including T_a , RH, clw, ciw, and C. Modnew was trained by the corresponding training samples at hourly and daily scales. Details of the development of the new model presented in the present study are given in Section 4.1.

3.2.2 Model performances evaluation

Table 4 lists the different cases for the R_i model comparison. As shown in Table 4, the nine evaluated models (Mod1–Mod8 and Modnew) were all used for clear-sky R_i estimation at both hourly and daily scales, while only four models (Mod6–Mod8 and Modnew) were evaluated under all-sky conditions. Three metrics were employed to present the model accuracy: R^2 , the root-mean-square error (RMSE), and bias. Generally, all three statistics were calculated to evaluate the accuracy of different models, but the RMSE values had larger weights.

Table 4
Detailed Information of the Six Cases Considered in the Model Evaluation

Case	Training samples	Validation samples	Evaluated model
Hourly Daytime		40,805	Mod1-Mod8, Modnew

		Nighttime	176,510	35,125	Mod1-Mod8, Modnew
Clear-sky	Daily		3,443	1,447	Mod1-Mod8, Modnew
	Hourly	Daytime	917,270	147,981	Mod6-8, Modnew
All-sky		Nighttime		210,057	Mod6-8, Modnew
	Daily		33,151	14,115	Mod6-8, Modnew

4 Results and Analysis

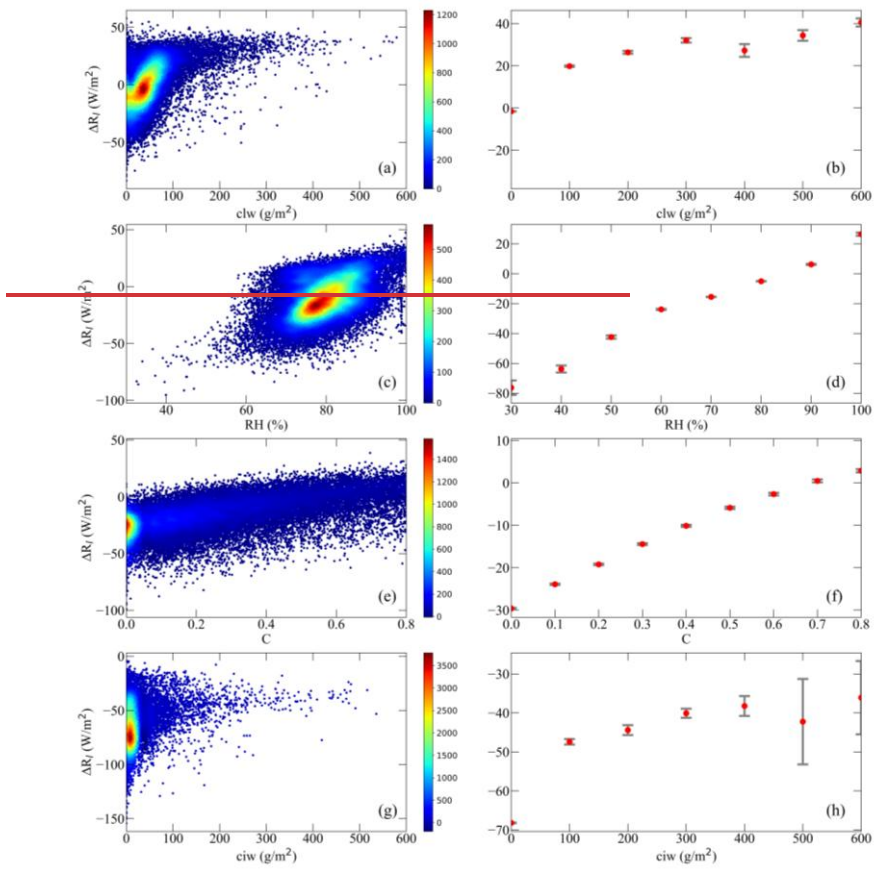
In this section, Modnew is introduced first, and then the validation results of the nine evaluated models under various cases are compared and analyzed. Lastly, further analyses are conducted on Modnew.

4.1 Modnew development

As mentioned above, the ocean-surface R_l in Modnew is related to five parameters (T_a , clw , RH , C , and ciw) for hourly and daily scales under all-sky conditions. To understand better the contribution made by each variable on R_l , the five parameters were introduced into Modnew gradually. Taking the daily all-sky R_l as an example, R_l was first only characterized by the fourth power of T_a based on the Stefan–Boltzmann law as follows:

$$R_l = a_{new} \sigma T_a^4 + b_{new} \quad (13)$$

where a_{new} and b_{new} are empirical coefficients, determined as 0.85 and 14.96, respectively, based on the daily training samples. Then, the correlations between the model residuals in R_l (referred to as ΔR_l) that define the difference between the in situ R_l measurements and the R_l estimates from Equation (13) and other four parameters (clw , RH , C , and ciw) were explored one by one. The results are found in Figure 2.



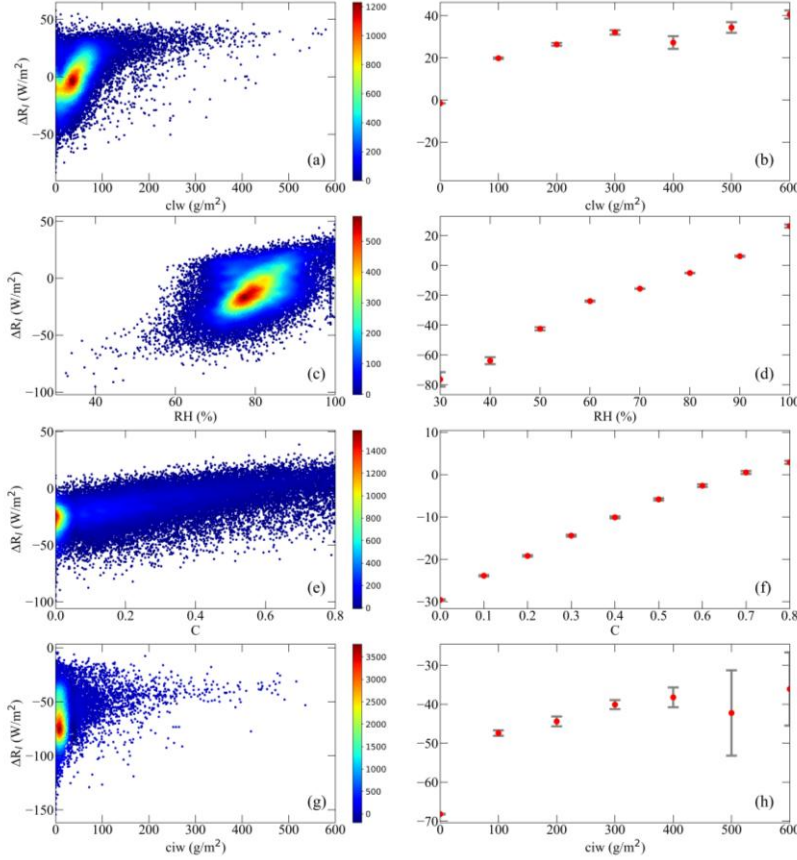


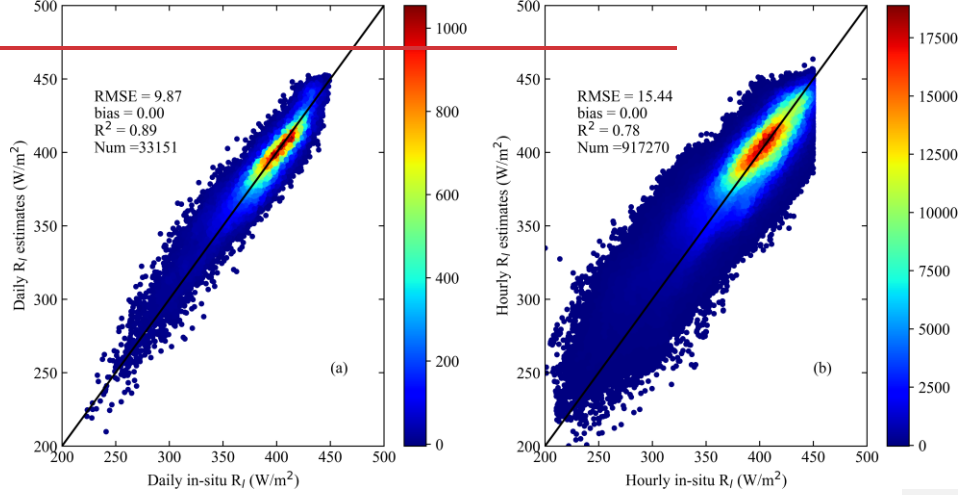
Figure 2. The scatter plots between the model residuals, ΔR_l , from Equation (13) and (a) clw, (c) RH, (e) C, and (g) ciw. Panels (b), (d), (f), and (h) are their corresponding box plots. In the left column, the color bar represents points per unit area. In the right column, the dots indicate the mean value of the ΔR_l (ME), while the vertical lines represent the standard error of the mean (SEM).

Figures 2(a), 2(c), 2(e), and 2(g) present scatter plots between ΔR_l and clw, RH, C, and ciw, respectively. In order to show their relationships better, the corresponding box plots, in which the mean of ΔR_l and its standard error (SEM) for each bin of the four parameters (in 10% increments) were calculated and presented in Figures 2(b), 2(d), 2(f), and 2(h), respectively. Specifically, ΔR_l varied with clw and ciw in a logarithmic relationship (Figures 2(b) and 2(h), respectively), and with RH (Figure 2(d)) and C (Figure 2(f)) in approximately linear relationships. We found that by introducing the C, RH, clw and ciw in Equation (13) gradually, the RMSE error was reduced from 17.48 W/m² with Equation (13) to 12.61 W/m², 10.92 W/m², 10.11 W/m² and 9.87 W/m², and the level of R^2 increased accordingly from 0.64 to 0.81, 0.86,

0.88 and 0.89, respectively. Hence, clw , RH , C , and ciw were introduced into Equation (13) in their appropriate forms and the final equation was taken as Modnew:

$$R_l = a_{new}\sigma T_a^4 + b_{new}C + c_{new} \ln(1 + clw) + d_{new} \ln(1 + ciw) + e_{new}RH + f_{new} \quad (14)$$

where a_{new} , b_{new} , c_{new} , d_{new} , e_{new} , and f_{new} are empirical coefficients. In this study, these coefficients were determined as 1.06, 39.054218, 4.910, -2.06497, 0.9189, and -177.53828 respectively. Figure 3(a) shows that the overall training accuracy of the estimated all-sky ocean-surface R_l from Modnew was satisfactory, yielding an R^2 of 0.89, RMSE of 9.9987 W/m^2 , and nearly no bias. Afterwards, Equation (14) was used to determine the hourly ocean-surface R_l based on the corresponding hourly training samples (see Table 4). The hourly results shown in Figure 3(b) were satisfactory, with an R^2 of 0.78, RMSE of 15.7244 W/m^2 , and nearly no bias. Note that the R_l measurements whose values were larger than $450 W/m^2$ were thought to be unreasonable and were manually removed (see Section 3.1).



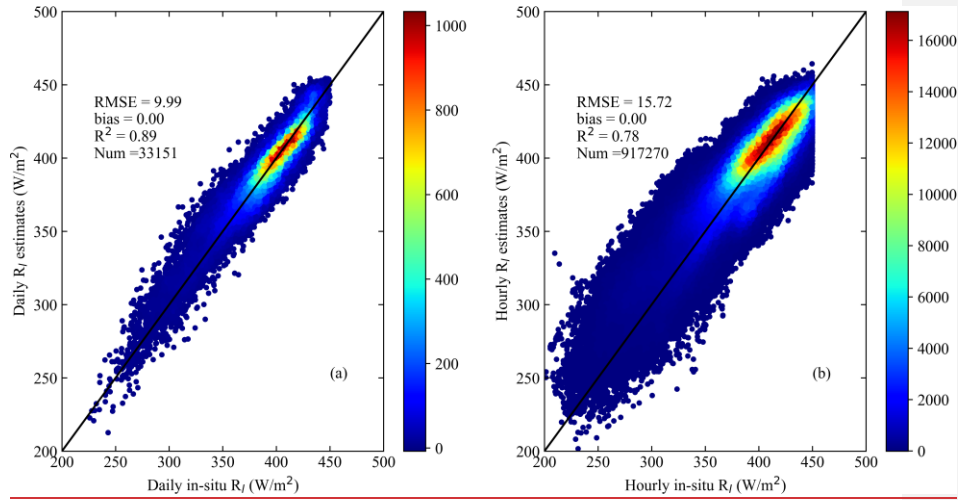


Figure 3. Overall training accuracy of the all-sky daily R_f at (a) daily and (b) hourly scales. In panels a and b, the color bar represents points per unit area.

By considering the influence of the calculated cloud cover on the R_f estimates, the hourly results were separated into daytime and nighttime, respectively, as shown in Figure 4. The training accuracy of the daytime sample was higher than that at nighttime, with R^2 values of 0.892 and 0.789 and RMSE values of 13.8818 and 16.284 W/m^2 , respectively. It was assumed that the larger uncertainties in the hourly ocean-surface R_f at nighttime were possibly owing to the estimated cloud cover, which might have an influence on Modnew in the form of overestimating R_f . Overall, the performance of Modnew was very good, both at daily and hourly scales for all-sky R_f estimation at the ocean surface.

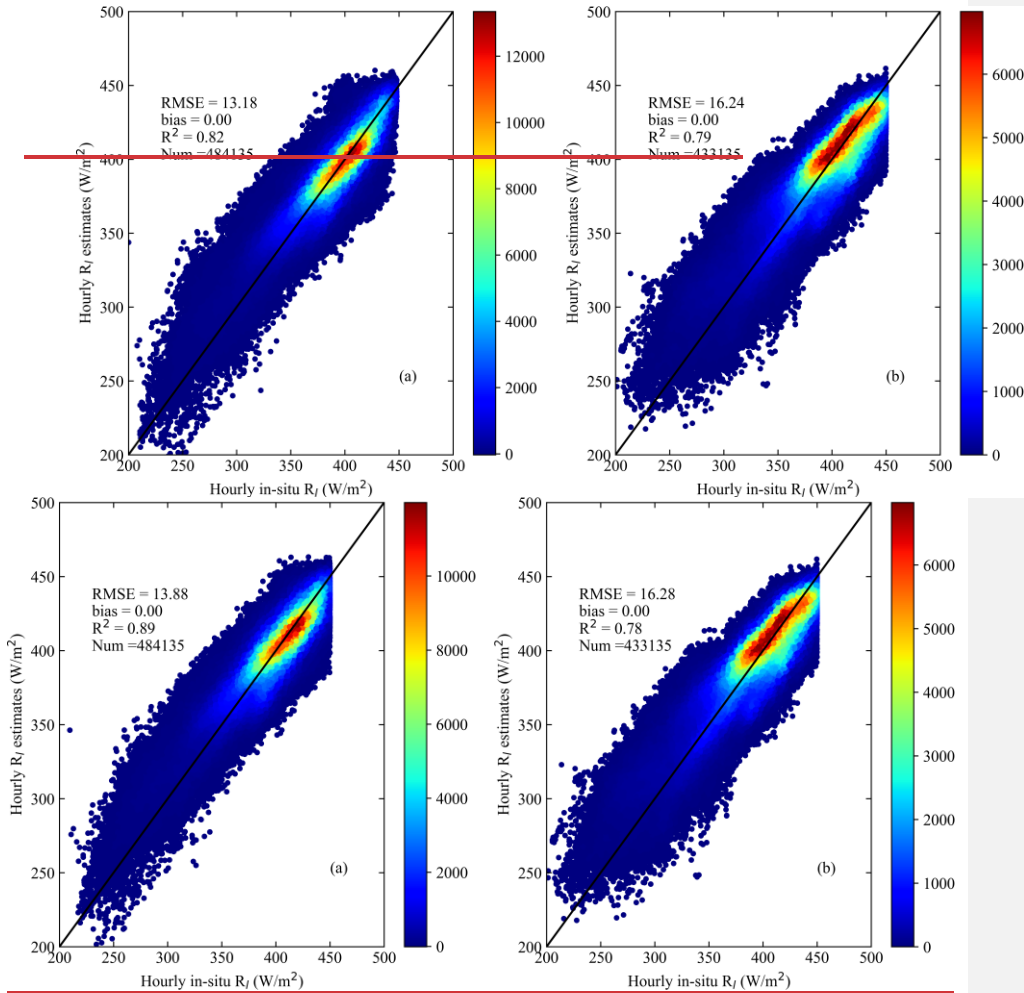


Figure 4. Overall training accuracy of the all-sky hourly R_f during (a) daytime and (b) nighttime. The color bars represent points per unit area.

4.2 Model comparison results

Based on the independent validation samples, Mod1–Mod8 and Modnew were validated one by one and compared for various cases (Table 4). Before that, the eight existing models were calibrated using the corresponding training samples, which means that Mod1–Mod5 were calibrated with the clear-sky training hourly/daily samples, while Mod6–Mod8 were calibrated with the all-sky training hourly/daily samples, i.e., the same as Modnew. Afterwards, these models were validated against the matched validation samples for each case. The updated

coefficients of Mod1–Mod8 and the coefficients of Modnew for hourly and daily scales are given in Table 5. For better illustration, the comparison results are presented for clear- and all-sky conditions in the following paragraphs.

Table 5
Coefficients of the Nine Models Used for Hourly/Daily Ocean-surface R_t Estimation. The Values in Parentheses are the Uncertainties of the Fitted Parameters

Models	a	b	c	d	e	f
Hourly						
Mod1	0.6475(±3.76 ×10 ⁻⁴)	0.0752(±1.53 ×10 ⁻⁴)	/	/	/	/
Mod2	0.2246(±2.12 ×10 ⁻⁴)	8.25777 ×10 ⁻⁴ (±0.013)	/	/	/	/
Mod3	1.234(±7.689 ×10 ⁻⁵)	/	/	/	/	/
Mod4	1.0856(±6.68 ×10 ⁻⁵)	/	/	/	/	/
Mod5	1.35748(±0.024)	2.73128(±0.0036)	0.5(±0.0045)	/	/	/
Mod6	0.28729(±1.44 ×10 ⁻⁴)	-0.02806(±2.858 ×10 ⁻⁵)	/	/	/	/
Mod7	0.82912(±2 ×10 ⁻⁴)	0.0021(±1.057 ×10 ⁻⁶)	0.066121(±5.874 ×10 ⁻⁴)	/	/	/
Mod8	-3.815557(±0.08338)	7.7313378(±0.081035)	-261.688243(±0.32124)	0.99085(±0.021)	256.678533(±0.03260)	/
Modnew	10.986(±36 ×10 ⁻⁴)	3040.991(±0.065)	3.993116(±0.0074)	-1.082.478(±0.0043)	0.9521(±0.012)	-145.964.62(±0.1430)
Daily						
Mod1	0.656(±0.004)	0.06(±0.001)	/	/	/	/
Mod2	0.225(±0.003)	7.3277 ×10 ⁻⁴ (±0.18)	/	/	/	/
Mod3	1.234(±5 ×10 ⁻⁴)	/	/	/	/	/
Mod4	1.07464(±5 ×10 ⁻⁴)	/	/	/	/	/
Mod5	1.9569(±0.09)	2.0267(±0.25)	0.5(±0.02)	/	/	/
Mod6	0.3286(±0.002)	-0.043(±3 ×10 ⁻⁴)	/	/	/	/
Mod7	0.742805(±0.002)	0.0042(±8 ×10 ⁻⁵)	0.133(±0.01)	/	/	/
Mod8	-0.1534(±0.02)	7.58545(±0.19)	-1112.19(±0.59)	0.058(±0.009)	0.058(±0.006)	/
Modnew	1.06(±0.002)	39.0542.18(±0.1722)	4.910(±0.056)	-2.061.97(±0.04)	0.9189(±0.008)	-1778.5328(±1.15)

4.2.1 Clear sky

All models, including the eight previous models (Mod1–Mod8), and the newly developed model (Modnew), could be used under clear-sky conditions at both hourly and daily scales with the updated coefficients given in Table 5.

4.2.1.1 Hourly scale

Table 6 shows the validation results of the nine models under clear-sky conditions at the hourly scale. Meanwhile, the validation results of Mod1–Mod8 with their original coefficients (see Section 2) are also presented in Table 6, using the same validation samples for comparison.

Table 6

Overall Validation Accuracy of the Nine Ocean-surface R_1 Models under Clear-sky Conditions at the Hourly Scale. The Values in Parentheses for Mod1–Mod8 are the Validation Results Found Using Their Original Coefficients

Models	R^2	RMSE(W/m ²)	bias(W/m ²)
Mod1	0.8077 (0.80078)	13.5714.69 (17.0115.43)	-0.43-0.42 (-9.49-0.88)
Mod2	0.741 (0.741)	15.3816.37 (19.0316.61)	-0.410.31 (-11.21-2.80)
Mod3	0.8077 (0.8077)	13.6514.77 (13.7417.87)	-0.6053 (1.349.84)
Mod4	0.774 (0.774)	14.4615.53 (14.5117.11)	-0.26-0.22 (-1.097.33)
Mod5	0.797 (0.8077)	13.6614.62 (15.4126.90)	-0.5244 (6.76-19.56)
Mod6	0.8075 (0.6777)	13.5816.87 (19.9321.51)	-0.457.33 (3.4215.28)
Mod7	0.8074 (0.8077)	13.4618.37 (22.5917.52)	-0.429.27 (-18.11-9.57)
Mod8	0.8078 (0.8178)	14.6915.59 (44.5237.00)	-0.062.45 (-41.7433.27)
Modnew	0.8279	13.4414.82	-1.904.40

The validation results illustrate that most models estimated the clear-sky hourly ocean-surface R_1 with a similar accuracy, with R^2 values ranging from 0.74 to 0.8279, RMSE values ranging from 13.4414.62 to 15.3816.37 W/m², and bias values ranging from -1.90.53 to -0.069.27 W/m² (Table 6). All eight existing models with the calibrated coefficients had a higher accuracy than those with the original coefficients ~~except Mod7~~; in particular, the RMSE of Mod8 decreased by ~3021 W/m². The magnitude of the bias of Mod1–Mod8 also decreased after recalibration, with the magnitudes of the biases of Mod1–Mod8 ~~being much smaller than those that of Mod6–Mod8 and Modnew, which were was trained with the all-sky hourly samples.~~ Among the ~~four all sky~~ nine models, the newly developed Modnew performed the best, with the largest R^2 of 0.8279, the smallest RMSE of 13.4414.82 W/m².

Then, the hourly validation results of the nine models were further examined using the daytime and nighttime values separately, which are shown in Figure 5. The performance of ~~most all models, including the five clear sky models (Mod1–Mod5) and one all sky model (Mod8), in~~ estimating the hourly clear-sky R_1 during the daytime was much better than that at nighttime, with RMSE values at daytime and nighttime ranging from ~12.0212.50 to 14.8615.06 W/m² and 14.3916.80 to 17.4919.50 W/m², respectively. ~~On the contrary, the performances of Mod6–Mod7 and Modnew were better at nighttime than that at daytime, with RMSE values at daytime and nighttime ranging from 15.00 to 19.20 W/m² and 14.40 to 16.60 W/m², respectively. Regarding the bias values, at nighttime, all five clear sky models had a significant underestimation problem (negative biases), while the all sky models had smaller bias values. This may be due to the uncertainty in the calculated CI at nighttime, which could influence the cloud determination and then R_1 .~~ In addition, among the five clear-sky models, Mod2 based only on air temperature shows the lowest accuracy in terms of RMSE during both daytime and nighttime. Among the nine models, Modnew had the most stable performance in hourly R_1 estimation under clear-sky conditions during both daytime and nighttime with similar RMSE values of 12.9915.03 and 14.3938 W/m², respectively, where in particular its nighttime R_1 estimation accuracy was the best among the nine models. ~~However, no accuracy improvement was found when training Mod6 through Modnew using only clear-sky hourly samples.~~

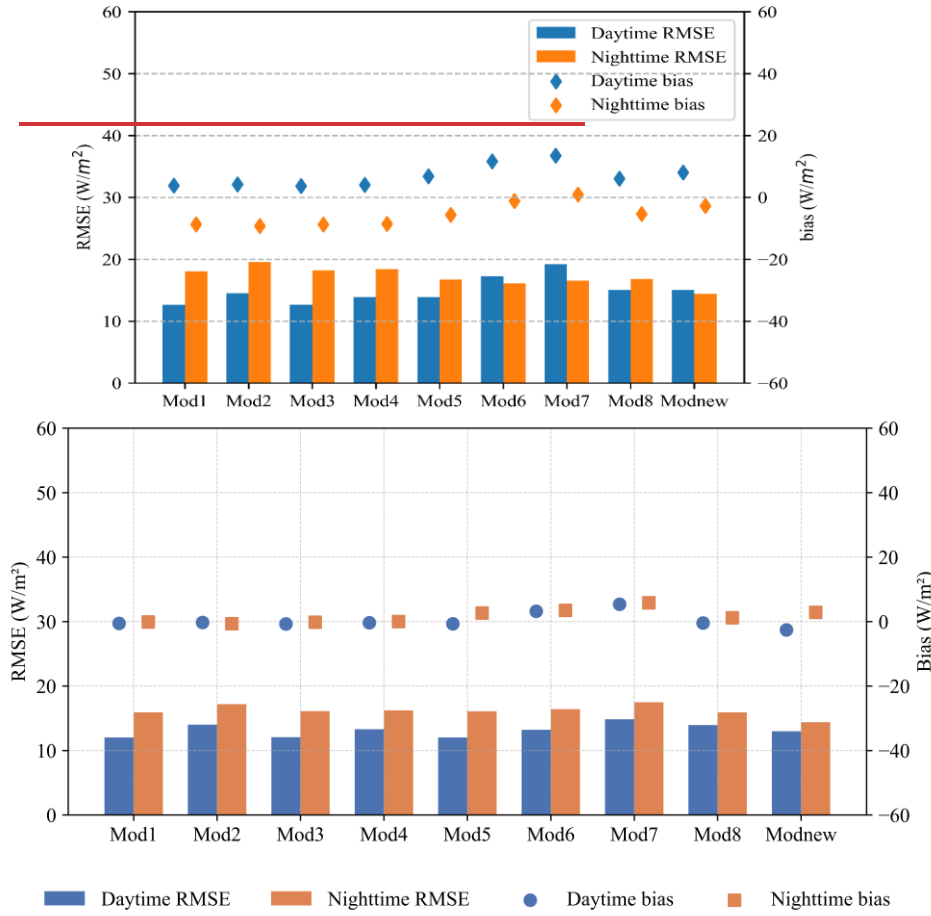


Figure 5. Validation accuracy of the estimated R_i under clear-sky conditions at the hourly scale for the nine models represented by RMSE (left axis) and bias (right axis).

Furthermore, the four all-sky R_i estimation models (Mod6–Mod8 and Modnew) were also trained using the clear sky hourly samples, and their outputs were validated against the in situ observations. The estimation accuracy of the four all-sky models all improved after calibration: their overall validated RMSE values decreased to ~ 13.40 to 15.40 W/m^2 and ~ 12.01 to 14.29 W/m^2 during the daytime, slight decreases (~ 1 W/m^2) at nighttime, and their biases values tended to 0. This indicates that the ability of the four all-sky models in estimating clear-sky hourly R_i was comparable with or even better than the other five models which only work for clear-sky conditions. Indeed, Modnew performed the best of all models during either daytime or nighttime, with corresponding validated RMSE values of 12.01 and 16.00 W/m^2 , respectively.

4.2.1.2 Daily scale

As for the results at the daily scale, the nine evaluated models were trained with the corresponding daily training samples (see Table 4) and validated against the in situ measurements. As shown in Table 7, the estimation accuracy of the daily clear-sky ocean-surface R_i from nearly all previous models improved significantly after recalibration, where the RMSE values and the magnitudes of the bias decreased by up to $\sim 4 \text{ W/m}^2$ and $\sim 109 \text{ W/m}^2$, respectively, except for Mod7. ~~The five clear-sky models (Mod1–Mod5) performed much better than the three previous all-sky models (Mod6–Mod8), with RMSE values ranging from 9.58 to 11.43 W/m^2 and 14.02 to 15.69 W/m^2 , and biases values ranging from 0.11 to 0.57 W/m^2 and 4.99 to 9.53 W/m^2 , respectively. Besides,~~ The Mod2 still exhibited lower accuracy than the other four clear-sky models, with the highest validated RMSE value of 11.5743 W/m^2 . The performance of Modnew was the best among the ~~four all-sky~~ nine models, with the smallest validated RMSE value of 8.3410.76 W/m^2 and bias of 0.593.53 W/m^2 . ~~Similar to the hourly results under the clear sky conditions, the validation results improved considerably if all four all-sky models were trained using the clear-sky daily samples: their RMSE values and biases decreased to 8–13 W/m^2 and were nearly zero, respectively, which were even better than the corresponding decreases measured for Mod1 to Mod5. Modnew was the best in comparison to the other three all-sky models, in this case yielding an RMSE of 8.36 W/m^2 . Similar to the results at the hourly scale, we did not observe accuracy improvements for Mod6 to Modnew when trained using only clear-sky daily samples.~~

Table 7
Overall Validation Accuracy of the Nine Ocean-surface R_i Models under Clear-sky Conditions at the Daily Scale. The Values in Parentheses for Mod1–Mod8 are the Validation Results Found Using Their Original Coefficients

Models	R^2	RMSE(W/m^2)	bias(W/m^2)
Mod1	0.89 (0.90)	9.7566 (12.7811.16)	0.318 (-6.69-2.00)
Mod2	0.85(0.85)	11.5743 (14.0111.91)	0.3645 (-8.04-3.35)
Mod3	0.90(0.90)	9.979.87 (10.9813.57)	0.0411 (4.369.06)
Mod4	0.88(0.88)	10.580 (10.8512.62)	0.4857 (2.457.16)
Mod5	0.89 (0.89)	9.6858 (9.9711.92)	0.339 (2.276.97)
Mod6	0.887 (0.88)	10.1614.32 (14.8118.43)	0.419.53 (10.6315.26)
Mod7	0.887 (0.88)	10.0014.02 (17.1513.67)	0.348.15 (-13.81-9.18)
Mod8	0.9080 (0.817)	10.5615.69 (37.4819.63)	0.684.99 (-34.9512.56)
Modnew	0.9289	8.3410.76	0.593.53

~~In summary, for the ocean-surface R_i estimation under clear-sky conditions, the use of an all-sky model trained with the clear-sky samples is recommended at both hourly and daily scales. Modnew performed the best of all nine models when trained with the clear-sky samples, and was comparable with the other five clear-sky models when trained with the all-sky samples. Furthermore, our validation results show that the accuracy of Mod2 is not as high as that of other clear-sky models that include water vapor variable in terms of RMSE.~~

4.2.2 All sky

4.2.2.1 Hourly scale

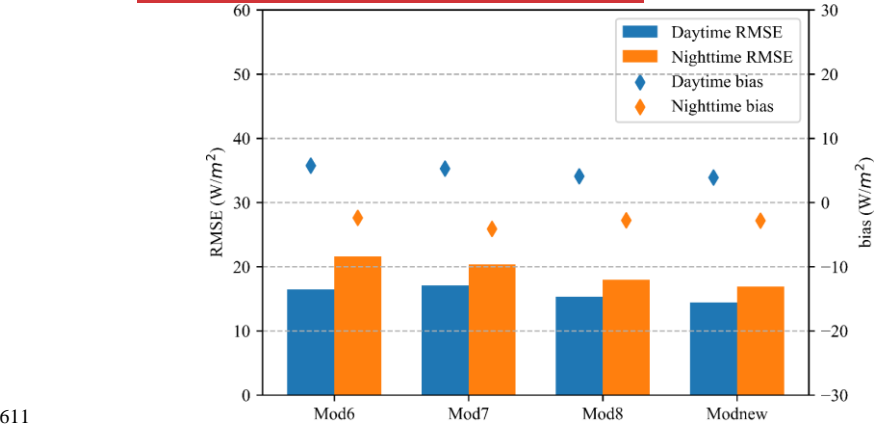
Table 8 gives the overall validation results of the all-sky hourly scale ocean-surface R_i from the four models against the independent validation samples with the updated and original

598 coefficients, respectively.

599 **Table 8**
600 *Overall Validation Accuracy of Four Ocean-surface R_1 Models under All-sky Conditions at the*
601 *Hourly Scale. The Values in Parentheses for Mod6–Mod8 are the Validation Results Found*
602 *Using Their Original Coefficients*

Models	R^2	RMSE(W/m ²)	bias(W/m ²)
Mod6	0.667 (0.635)	19.0718.53 (27.9419.84)	1.170.05 (-14.053.83)
Mod7	0.686 (0.6864)	18.3919.06 (19.8026.10)	-0.13-0.14 (3.45-10.27)
Mod8	0.74 (0.4851)	16.6691 (40.7437.33)	0.11-0.41 (-32.2528.47)
Modnew	0.776	15.6495	-0.04

603 Compared to the results in Table 6, the estimation accuracies under all-sky conditions
604 shown in Table 8 were generally worse, with lower R^2 values (0.66–0.776) and bigger RMSE
605 values (15.6495–19.076 W/m²), which indicates that the uncertainty in the cloud information
606 was the major reason for the increased uncertainty in the R_1 estimation. As in previous results,
607 the three previous models, Mod6–Mod8, performed much better after recalibration, with
608 decreased RMSE values up to ~20–24 W/m² and their bias values tended to 0: ~~Mod7 still~~
609 ~~performed the worse~~. Modnew performed the best, with an RMSE of 15.6495 W/m² and a bias of
610 -0.04W/m², followed by Mod8.



611

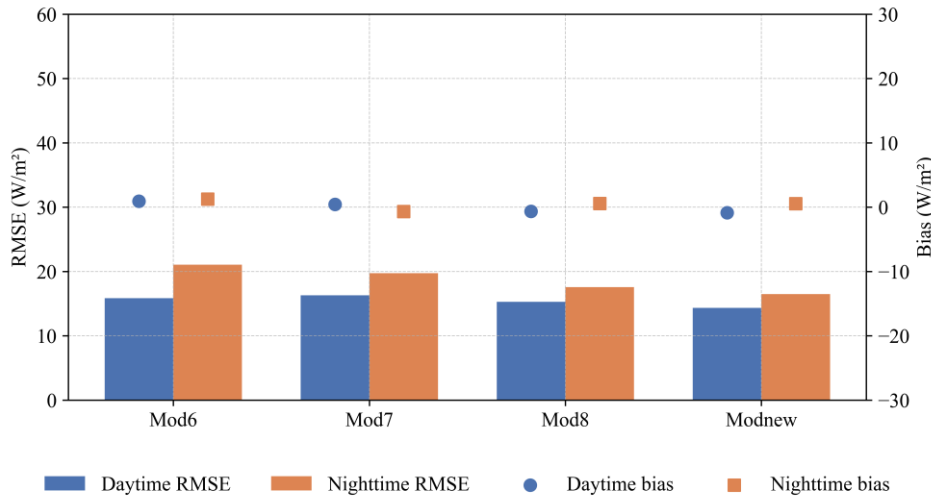


Figure 6. Validation accuracy of the estimated RI under all-sky conditions at the hourly scale for Mod6-Mod8 and Modnew represented by RMSE (left axis) and bias (right axis).

The hourly results in Table 8 were examined for daytime and nighttime values, as shown in Figure 6. The results show that the estimation accuracies of the four models were overall better during the daytime than at nighttime, with smaller RMSE values for the former. Specifically, during daytime hours, the accuracy of Modnew was similar to that of Mod8, with RMSEs of 14.3443 and 15.2933 W/m², respectively, which were better than those of Mod6 and Mod7, which yielded RMSEs of 15.85+6.46 and 16.30+7.09 W/m², respectively. However, Mod7 performed a little bit better than Mod6 during the nighttime, although its overall performance was the worst. It is speculated that the larger uncertainties in the all-sky ocean-surface R_i values at nighttime can possibly be attributed to the cloud information at nighttime, which was difficult to estimate accurately compared to the daytime cloud information.

4.2.2.2 Daily scale

Figure 7 shows the overall validation accuracies of the all-sky daily ocean-surface R_i values from the four models. Compared with Mod6-Mod8, Modnew had the best performance, with a validated RMSE of 10.27 W/m², a bias of 0.10 W/m², and an R² of 0.88, followed by Mod8, which yielded an RMSE of 11.96 W/m², a bias of -0.18 W/m², and an R² of 0.85. However, Mod8 had a tendency to overestimate low values (<300 W/m²), as did Mod6 and Mod7.

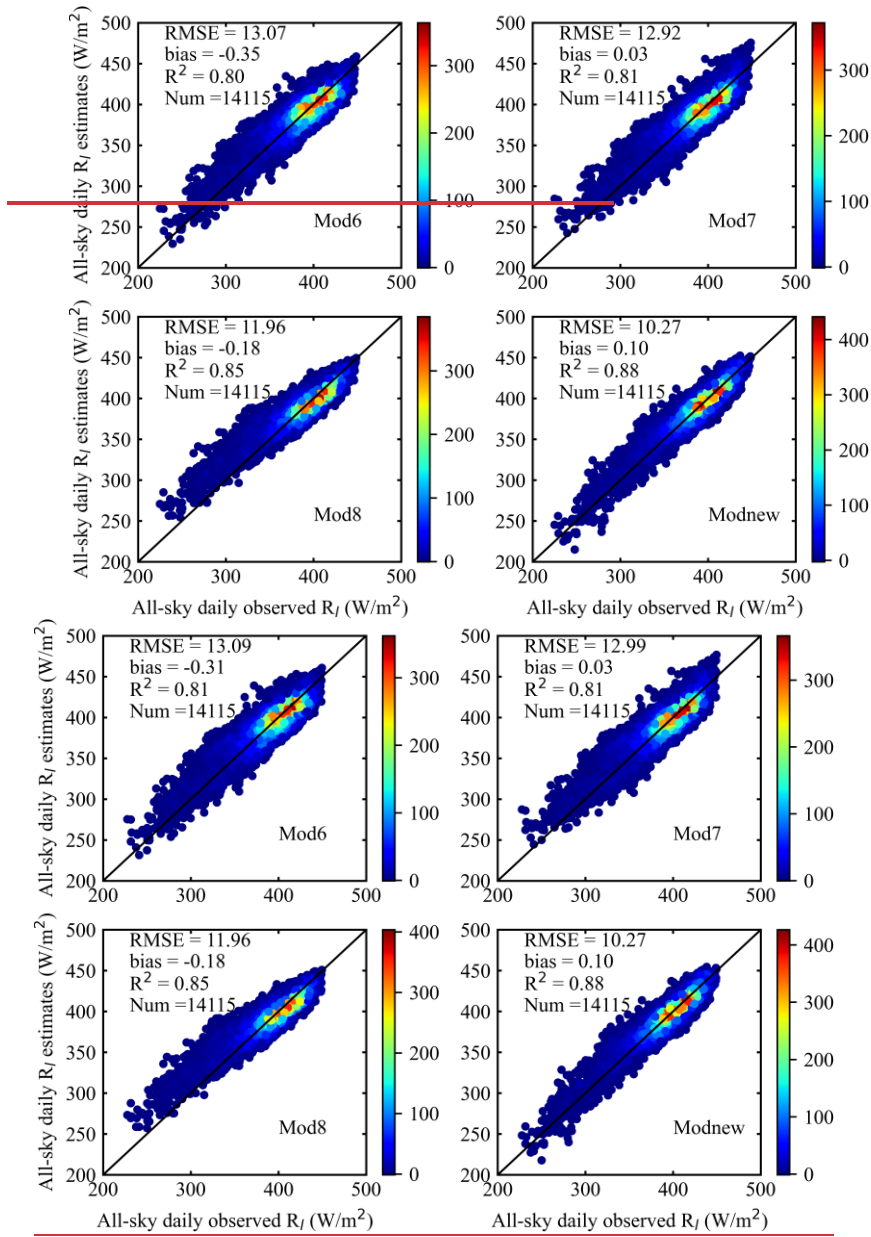


Figure 7. Overall validation result of the calculated all-sky daily ocean-surface R_f from the four

models against the independent moored measurements. The color bars represent points per unit area.

Overall, it is speculated that Modnew performed better than Mod6–Mod8 because of the introduction of two cloud-related parameters (clw and ciw) into the model in addition to the cloud fraction. In order to demonstrate this speculation better, the relationship between the estimation errors in the daily all-sky ocean-surface R_1 of the four models and clw, which was used to represent the CBH, was further analyzed. The corresponding mean of the estimation errors in the daily all-sky ocean-surface R_1 and its SEM for each bin of clw in logarithmic format (in 10% increments) were calculated, as presented in Figure 8.

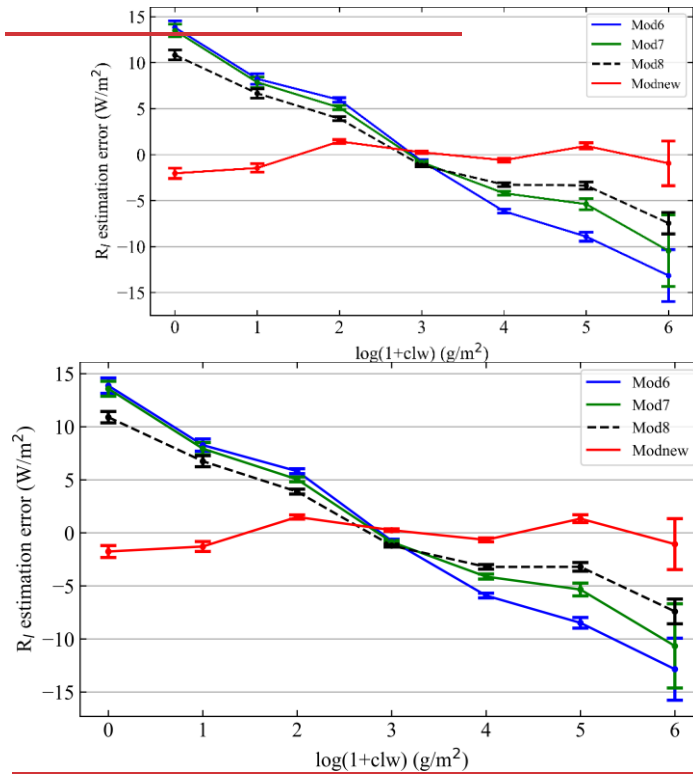


Figure 8. The averaged R_1 estimation errors and its SEM of Mod6 – Mod8 and Modnew varied with clw in logarithmic format.

From the results in Figure 8 it can be seen that the R_1 estimation errors of Mod6–Mod8 were negative linearly related to increasing $\log(1+\text{clw})$; such behavior is not seen for Modnew. This indicates that the cloud information related to the variations in daily ocean-surface R_1 are not fully characterized by only the cloud fraction. Although Mod8 performed better than Mod6 and Mod7 because of the introduction of the dew point depression to compensate for the

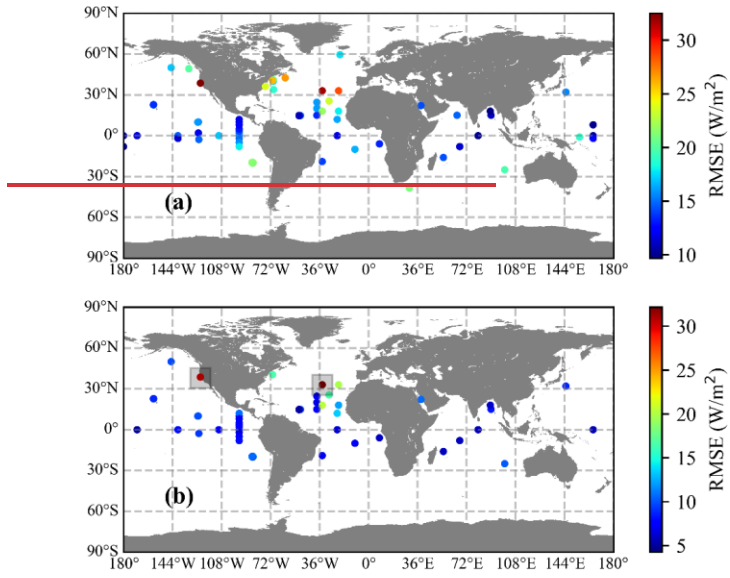
653 difference between the surface temperature and cloud base temperature, the contributions of the
654 cloud base emission to R_1 still cannot be thoroughly expressed over the ocean surface. Hence,
655 Modnew performed superior to other models because it also takes clw as input. Moreover, ciw
656 was also introduced in Modnew to ensure its robust performance at high latitudes.

657 4.3 Further analysis on Modnew

658 Based on the direct validation results described above, Modnew satisfactorily estimated
659 the ocean-surface R_1 under both clear- and all-sky conditions at both hourly and daily scales.
660 Hence, further analysis of this new model, such as testing its performance robustness and a
661 sensitivity analysis, was conducted, and the results are given below.

662 4.3.1 Modnew performance analysis

663 In order to examine the robustness of its performance, the spatial distributions of the
664 validation accuracies of the all-sky R_1 estimates from Modnew at the moored buoy sites are
665 presented in Figures 9(a–b) for hourly and daily scales, respectively. Note that the moored buoy
666 data from which the number of provided validation samples were less than 50 were excluded to
667 provide a more objective comparison.



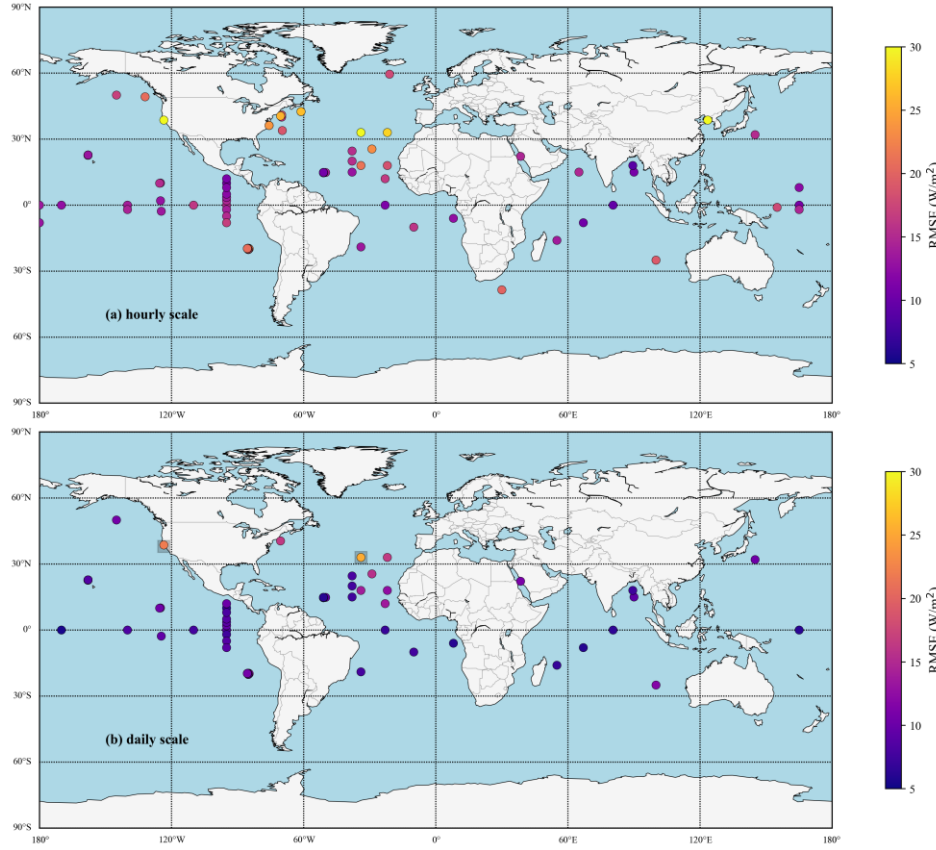
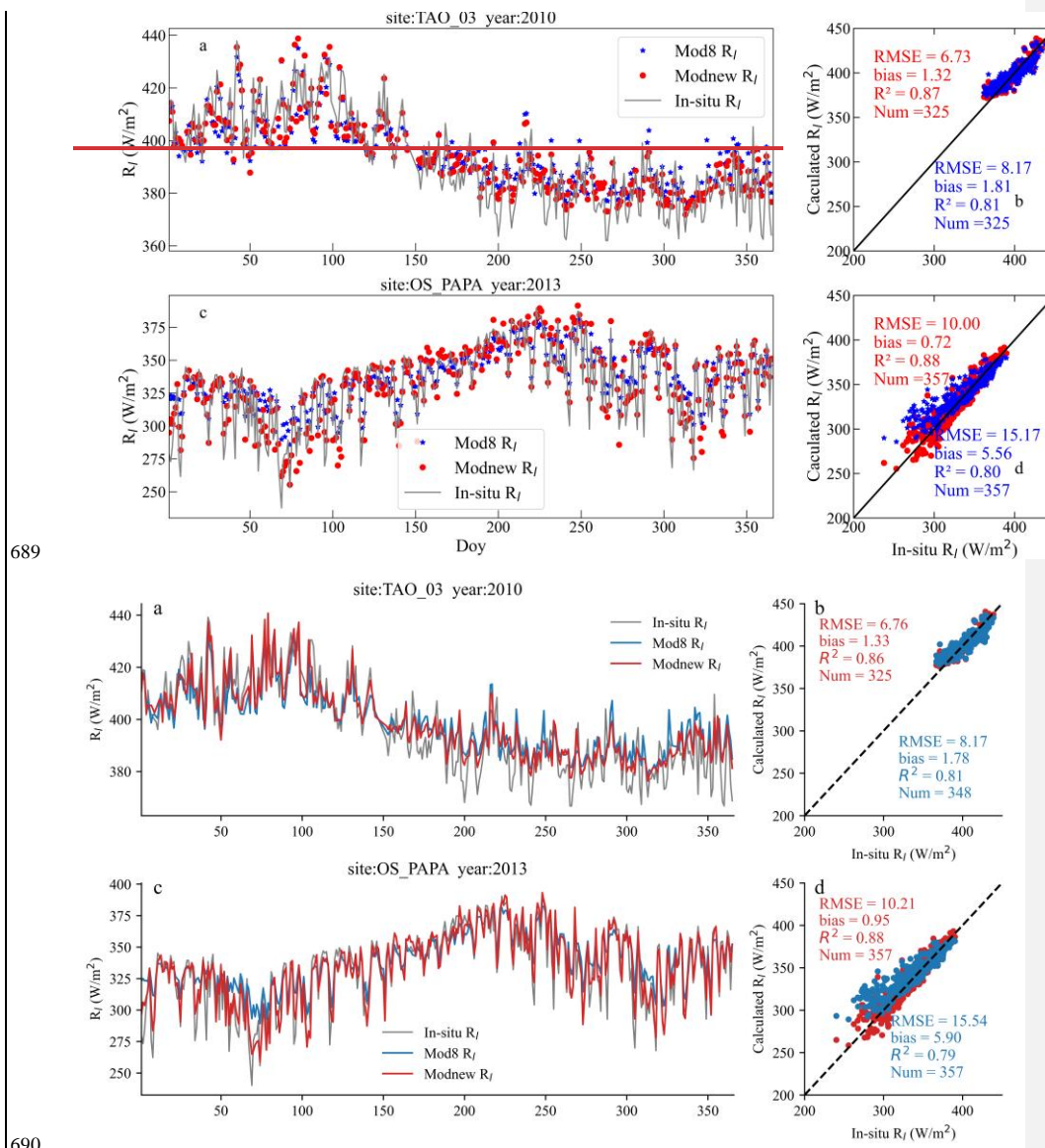


Figure 9. Validation accuracies of Modnew on the hourly scale (a) and daily scale (b) at different sites represented by the RMSE values. The two moored buoys in the shaded boxes in (b) are UOP_SMILE88 (38°N, 123.5°W) and UOP_SUB_NW (33°N, 34°W).

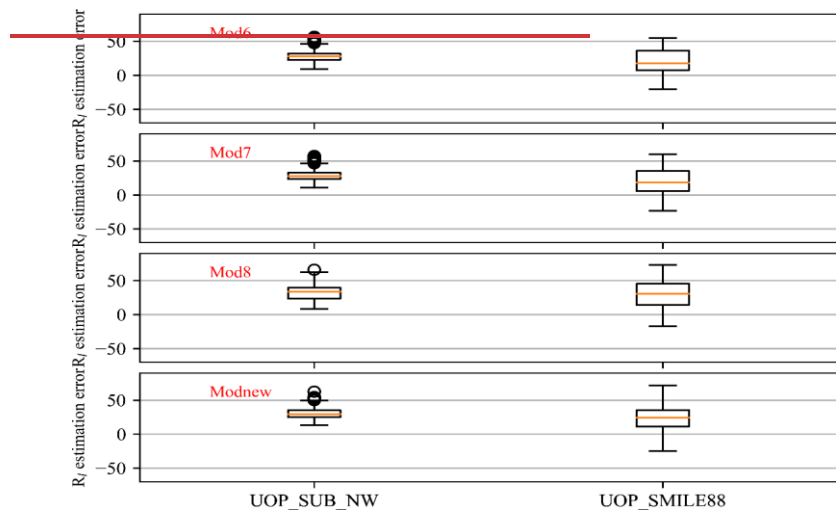
The spatial distribution of the validation accuracy (represented by RMSE) of the R_i estimates from Modnew was similar for the hourly and daily data. Their RMSE values got larger from tropical to the high latitude seas, although the daily R_i estimates were generally more accurate than the hourly ones, and the validation accuracy for sites at open seas was more accurate than that within coastal seas. For a better illustration, two time series of the estimated daily ocean-surface R_i from Modnew at two sites were randomly selected and shown in Figure 10, and the one from Mod8 was added for comparison, as well as the corresponding scatter plots. The two buoys, TAO_03 (0°N, 140°W) and OS_PAPA (50°N, 145°W), are in equatorial and mid-high latitude seas, respectively. The temporal variations in the all-sky daily R_i estimates from the two models both captured the variations in the moored R_i measurements very well, but the ones from Modnew were closer to the measurements at high values and low values,

684 especially at the OS_PAPA site. The validation accuracy of Modnew was higher than that of
 685 Mod8 at both sites, and Modnew performed better for tropical seas, with validated RMSE values
 686 of 6.76 and 10.21 W/m^2 , respectively, which was assumed that more samples used for
 687 modeling were collected at tropical seas and this would influence the model performance at mid-
 688 high latitude seas.



691 **Figure 10.** Time series and scatter plots of the R_l estimates and the moored R_l measurements at
 692 the (a–b) TAO_03 (0°N, 140°W) and (c–d) OS_PAPA (50°N, 145°W) sites. The red points and
 693 blue points represent Modnew and Mod8, respectively.

694 However, it was noted that Modnew performed poor at some sites, such as
 695 UOP_SMILE88 (38°N, 123.5°W) and UOP_SUB_NW (33°N, 34°W) (see the shaded boxes in
 696 Figure 9). The estimation errors in the daily R_l from Modnew at the two moored buoys were
 697 calculated, as shown in Figure 11, and the ones from the other three all-sky models, Mod6–
 698 Mod8, are shown for comparison. It can be seen that the four evaluated all-sky models all
 699 worked poorly at the two sites, all giving overestimations. A possible explanation may be
 700 attributed to the differences in the characteristics of the atmospheric boundary layer over the two
 701 sites relative to the open sea. Specifically, UOP_SMILE88 is deployed on the northern California
 702 shelf, which is influenced by air temperature inversions (ATIs) (Dorman et al., 1995), and
 703 UOP_SUB_NW is deployed near the eastern flank of the Azores anticyclone system (Moyer &
 704 Weller, 1997). As such, the atmospheric conditions of the two sites are different from those over
 705 the open sea, which would affect the estimation of R_l made with models whose coefficients were
 706 determined by samples collected mostly from sites located in the open sea. Therefore, more
 707 samples should be collected within these seas to help to improve the ocean-surface R_l estimation
 708 accuracy in these areas.



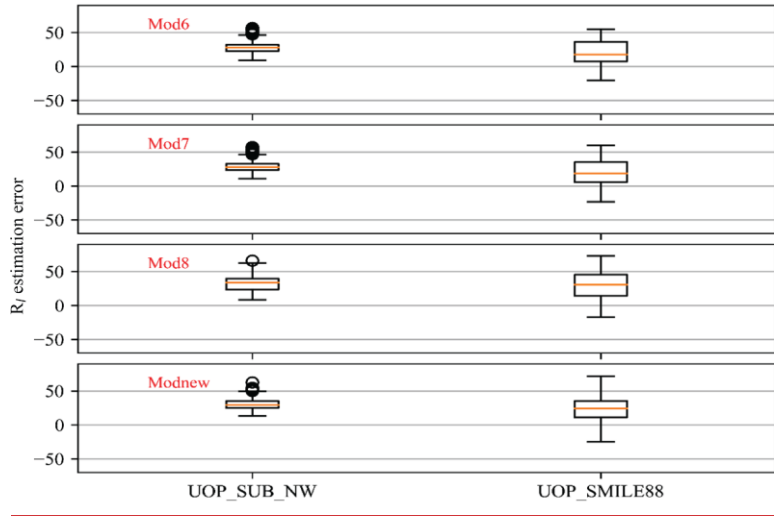


Figure 11. Box plots of the R_1 estimation errors from models Mod6, Mod7, Mod8, and Modnew at UOP_SMILE88 (38°N, 123.5°W) and UOP_SUB_NW (33°N, 34°W). The top edge, center, and bottom edge of the box represent the 75th, 50th (median), and 25th percentiles, respectively. The whiskers indicate the maximum and minimum values within 1.5 times the interquartile range (IQR), and the circles denote outliers.

4.3.2 Sensitivity analysis

In order to quantify the impact of each parameter on the calculated R_1 in Modnew, the SimLab software (<http://simlab.jrc.ec.europa.eu>) was used to conduct a global sensitivity analysis. All inputs in Modnew (T_a , RH, C, clw, and ciw) were entered into the software separately, and then 2,000 ocean-surface R_1 values were calculated using Modnew by taking 2,000 combinations of these parameters as inputs. Afterwards, the Fourier amplitude sensitivity test (FAST) method (Saltelli et al., 1999) in the SimLab software was employed to conduct a sensitivity analysis based on the inputs, and the corresponding estimated R_1 values were used for a sensitivity analysis using the total sensitivity index (TSI). The TSI indicates each parameter's total contribution to the output variance when the interactions of other parameters are also considered, and was used to quantify the sensitivity of each parameter. Table 9 shows the TSI of each parameter in Modnew. Specifically, T_a had the most important effect on R_1 with the largest TSI of 41.26%, followed by C (25.6%) and RH (21%). Therefore, the performance of Modnew mainly depended on the accuracy of the T_a , C, and RH. The TSI of clw was the fourth highest with 8%, but it is essential to supplement cloud information that cloud cover alone cannot provide, especially for cloud-sky conditions. In terms of ciw, its TSI was just 0.008, which was possibly because only a few samples at high-latitudes were used in this study.

Table 9

FAST Sensitivity Indices of the First Order for Each Input Variable in Modnew

T_a	RH	C	Clw	ciw
0.4126	0.21	0.256	0.08	0.008

5 Conclusions

Due to the significance of R_l at the ocean surface, many empirical models have been established for ocean-surface R_l calculation based on observations by relating R_l to some climatic factors, such as T_a , RH, and so on. However, most models were developed only for clear days, and for those models that can calculate the all-sky R_l , only the cloud cover is taken into account, which is thought to be insufficient for characterizing the influence of clouds on R_l , especially for ocean surfaces where cloudy skies are common. Indeed, most previous R_l estimation models were developed only within a specific region based on limited observations, and some for just land surfaces. Consequently, there was a need to perform comprehensive evaluations of these models, including their ability to predict R_l over global seas.

In this study, ~~a new model called Modnew, in which the all-sky ocean-surface R_l is nonlinearly related to T_a , RH, C, clw, and ciw, has been successfully developed. the newly developed Modnew model estimates all-sky ocean-surface downward longwave radiation (R_l) by incorporating key atmospheric and cloud parameters: screen-level air temperature (T_a), relative humidity (RH), fractional cloud cover (C), total column cloud liquid water (clw), and total column cloud ice water (ciw). T_a governs the thermal radiation emitted by the atmosphere, as described by the Stefan–Boltzmann law. RH modifies the atmospheric emissivity by representing the water vapor content. C quantifies the cloud's overall presence, while clw and ciw capture the thermal contributions of liquid and ice clouds, respectively, enabling a more accurate characterization of cloud radiative effects. The Modnew model relies on specific atmospheric and cloud-related parameters for accurate R_l estimation. While inputs such as T_a and RH are commonly obtained from in situ measurements, critical cloud-related parameters (i.e. clw and ciw) are typically derived from satellite products or reanalysis datasets, such as ERA5. These parameters are essential for capturing the radiative properties of clouds, which in situ measurements alone cannot reliably provide. Therefore, satellite data or reanalysis products are indispensable for supplying these inputs.~~ This model, as well as eight comparison models, was used to estimate the all-sky ocean-surface R_l at both hourly and daily scales based on comprehensive observations collected from 65 globally distributed moored buoys from 1988 to 2019. In contrast to previous models, Modnew incorporates more cloud-related parameters (i.e., clw and ciw) into the model besides just cloud cover. Modnew and the eight previous R_l models were assessed against the moored values for various cases, including clear- and all-sky conditions at daytime and nighttime and at hourly and daily scales. After careful analysis, several major conclusions could be drawn, as follows:

(1) The eight previous models performed much better after calibration of their coefficients with the global observations for almost all cases, except Mod7 in some situations.

(2) For the clear-sky ocean-surface R_l estimation, ~~the four all-sky models (Mod6–Mod8 and Modnew) could work comparably to or even better than the five clear-sky models (Mod1–Mod5) if their coefficients were calibrated by the clear-sky samples, yielding overall validated RMSE values ranging from 13.40 to 15.40 W/m^2 at the hourly scale and 8.00–13.00 W/m^2 at the daily scale. In terms of daytime and nighttime, all five clear-sky models (Mod1–Mod5) performed better at daytime than that at nighttime, and vice versa for the four all-sky models~~

except Mod7. Mod1–Mod5 generally had the tendency to underestimate R_i at nighttime because they do not consider the influence of clouds. Among all models, Modnew was the most robust, yielding RMSE values of 12.99 ± 5.03 W/m² and 14.39 W/m² at daytime and nighttime for the hourly scale, respectively.

(3) For the all-sky ocean-surface R_i estimation, the performance of the four evaluated models was generally worse compared to that under clear-sky conditions, which further demonstrated that the uncertainty in the all-sky R_i estimation was highly dependent on accurate cloud information. Specifically, at the hourly scale, the validated RMSE values of the four models ranged from 15.64 ± 5.95 to 19.07 W/m², with better performance at daytime. At the daily scale, the RMSE values ranged from 10.27 to 13.09 W/m². Modnew also performed the best in these cases, with an overall validated RMSE of 15.64 ± 5.95 and 10.27 W/m² and bias values of -0.04 and 0.10 W/m², respectively. It is worth noting that Modnew performed similarly during both daytime and nighttime at the hourly scale.

In summary, the performance of Modnew was superior to other previous models for ocean-surface R_i estimation for any case, which was mainly because of the introduction of more cloud-related information (clw and ciw). Further analysis of Modnew illustrated the significance of the two parameters as well as cloud cover. However, all results again emphasized that the accuracy of nearly all the empirical models was highly dependent on the spatial distribution, quality, and quantity of the samples used for modeling. For instance, Modnew worked better at open seas in tropical regions where more samples were available compared to other regions. Therefore, many more samples at different regions, such as in coastal regions and high-latitude seas, should be collected in the future to improve model performance. Moreover, more accurate cloud information especially at nighttime is essential to decrease the uncertainty in the estimated R_i at the ocean surface.

Competing interests

The contact author has declared that none of the authors has any competing interests.

Acknowledgments

We acknowledge the buoy data sets provided by UOP, GTMBA, and OceanSITES project. We are grateful to ECMWF for providing the reanalysis data sets. We would also like to thank the contributions made by the anonymous reviewers and editor that helped improve the quality of this paper.

Funding

This work was supported by the Natural Science Foundation of China (41971291).

Data availability

All data sets used in this research, including the moored buoy observations and satellite and reanalysis data are publicly available. Detailed information on these data sets, including

813 citations and web links, is presented in Section 3.

814 Author contributions.

815 PJH and BJ designed and performed the study. All authors contributed to the analysis of
816 results and final version of the paper.

817 References

- 818 Aase, J. K., & S. B. Idso (1978), A comparison of two formula types for calculating long-wave radiation from the
819 atmosphere, *Water Resour Res*, 14(4), 623-625, <https://doi.org/10.1029/WR014i004p00623>.
- 820 Alados, I., I. Foyo-Moreno, & L. Alados-Arboledas (2012), Estimation of downwelling longwave irradiance under
821 all-sky conditions, *Int J Climatol*, 32(5), 781-793, <https://doi.org/10.1002/joc.2307>.
- 822 Alappattu, D. P., Q. Wang, R. Yamaguchi, R. J. Lind, M. Reynolds, & A. J. Christman (2017), Warm layer and cool
823 skin corrections for bulk water temperature measurements for air-sea interaction studies, *J Geophys Res-Oceans*,
824 122(8), 6470-6481, <https://doi.org/10.1002/2017jc012688>.
- 825 Bignami, F., S. Marullo, R. Santoleri, & M. E. Schiano (1995), Longwave radiation budget in the Mediterranean
826 Sea, *J Geophys Res-Oceans*, 100(C2), 2501-2514, <https://doi.org/10.1029/94jc02496>.
- 827 Bilbao, J., & A. H. de Miguel (2007), Estimation of Daylight Downward Longwave Atmospheric Irradiance under
828 Clear-Sky and All-Sky Conditions, *J. Appl. Meteor. Climatol.*, 46(6), 878-889, <https://doi.org/10.1175/jam2503.1>.
- 829 Bourlès, B., R. Lumpkin, M. J. McPhaden, F. Hernandez, P. Nobre, E. Campos, et al. (2008), The PIRATA
830 program: History, accomplishments, and future directions, *Bull. Amer. Meteor. Soc.*, 89(8), 1111-1126,
831 <https://doi.org/10.1175/2008bams2462.1>.
- 832 Brunt, D. (1932), Notes on radiation in the atmosphere, *Quart J Roy Meteor Soc*, 58, 389-420.
- 833 Brutsaert, W. (1975), On a derivable formula for longwave radiation from clear skies, *Water Resour Res*, 11(5),
834 742-744, <https://doi.org/10.1029/WR011i005p00742>.
- 835 Buck, A. L. (1981), New equations for computing vapor pressure and enhancement factor, *J Appl Meteorol*, 20(12),
836 1527-1532, [https://doi.org/10.1175/1520-0450\(1981\)020<1527:NEFCVP>2.0.CO;2](https://doi.org/10.1175/1520-0450(1981)020<1527:NEFCVP>2.0.CO;2).
- 837 Caniaux, G. (2005), A 1 year sea surface heat budget in the northeastern Atlantic basin during the POMME
838 experiment: 1. Flux estimates, *J. Geophys. Res.*, 110(C7), <https://doi.org/10.1029/2004jc002596>.
- 839 Centurioni, L. R., J. Turton, R. Lumpkin, L. Braasch, G. Brassington, Y. Chao, et al. (2019), Global in situ
840 observations of essential climate and ocean variables at the air-sea interface, *Front Mar Sci*, 6, 419,
841 <https://doi.org/10.3389/fmars.2019.00419>.
- 842 Clark, N. E., L. Eber, R. M. Laurs, J. A. Renner, & J. F. T. Saur (1974), Heat exchange between ocean and
843 atmosphere in the eastern North Pacific for 1961-71, *Tech. Rep. NMFS SSRF-682*, NOAA, U.S. Dept. of Commer.,
844 Washington, D. C.
- 845 Cleugh, H. A., R. Leuning, Q. Mu, & S. W. Running (2007), Regional evaporation estimates from flux tower and
846 MODIS satellite data, *Remote Sens Environ*, 106(3), 285-304, <https://doi.org/10.1016/j.rse.2006.07.007>.
- 847 Cottier, F. R., F. Nilsen, M. E. Inall, S. Gerland, V. Tverberg, & H. Svendsen (2007), Wintertime warming of an
848 Arctic shelf in response to large-scale atmospheric circulation, *Geophys Res Lett*, 34(10),
849 <https://doi.org/10.1029/2007GL029948>.
- 850 Cronin, M. F., C. L. Gentemann, J. Edson, I. Ueki, M. Bourassa, S. Brown, et al. (2019), Air-sea fluxes with a focus
851 on heat and momentum, *Front Mar Sci*, 6, <https://doi.org/10.3389/fmars.2019.00430>.
- 852 Deremble, B., N. Wienders, & W. K. Dewar (2013), CheapAML: A simple, atmospheric boundary layer model for
853 use in ocean-only model calculations, *Mon. Wea. Rev.*, 141(2), 809-821, <https://doi.org/10.1175/MWR-D-11-00254.1>.
- 854 Diak, G. R., W. L. Bland, J. R. Mecikalski, & M. C. Anderson (2000), Satellite-based estimates of longwave
855 radiation for agricultural applications, *Agr Forest Meteorol*, 103(4), 349-355, [https://doi.org/10.1016/S0168-1923\(00\)00141-6](https://doi.org/10.1016/S0168-1923(00)00141-6).
- 856 Doelling, D. R., N. G. Loeb, D. F. Keyes, M. L. Nordeen, D. Morstad, C. Nguyen, et al. (2013), Geostationary
857 enhanced temporal interpolation for CERES flux products, *J. Atmos. Oceanic Technol.*, 30(6), 1072-1090,
859 <https://doi.org/10.1175/JTECH-D-12-00136.1>.
- 860

Field Code Changed

Field Code Changed

Donlon, C. J., P. J. Minnett, C. Gentemann, T. J. Nightingale, I. J. Barton, B. Ward, & M. J. Murray (2002), Toward improved validation of satellite sea surface skin temperature measurements for climate research, *J. Climate*, 15(4), 353-369, [https://doi.org/10.1175/1520-0442\(2002\)015<0353:tivoss>2.0.co;2](https://doi.org/10.1175/1520-0442(2002)015<0353:tivoss>2.0.co;2)

Dorman, C. E., A. G. Enriquez, & C. A. Friehe (1995), Structure of the lower atmosphere over the northern California coast during winter, *Mon. Wea. Rev.*, 123(8), 2384-2404, [https://doi.org/10.1175/1520-0493\(1995\)123<2384:SOTLAO>2.0.CO;2](https://doi.org/10.1175/1520-0493(1995)123<2384:SOTLAO>2.0.CO;2).

Douville, H., J. F. Royer, & J. F. Mahfouf (1995), A new snow parameterization for the Meteo-France climate model, *Climate Dynam.*, 12(1), 21-35, <https://doi.org/10.1007/BF00208760>.

Dubois, C., S. Somot, S. Calmanti, A. Carillo, M. Déqué, A. Dell'Aquila, et al. (2012), Future projections of the surface heat and water budgets of the Mediterranean Sea in an ensemble of coupled atmosphere-ocean regional climate models, *Climate Dynam.*, 39(7), 1859-1884, <https://doi.org/10.1007/s00382-011-1261-4>.

Ellingson, R. G. (1995), Surface longwave fluxes from satellite observations: A critical review, *Remote Sens Environ.*, 51(1), 89-97, [https://doi.org/10.1016/0034-4257\(94\)00067-W](https://doi.org/10.1016/0034-4257(94)00067-W).

Fasullo, J. T., J. Kiehl, K. E. Trenberth, & J. T. Fasullo (2009), Earth's Global Energy Budget, *Bull. Amer. Meteor. Soc.*, 90(3), 311-324, <https://doi.org/10.1175/2008BAMS2634.1>
info:doi/10.1175/2008BAMS2634.1.

Flerchinger, G. N., W. Xao, D. Marks, T. J. Sauer, & Q. Yu (2009), Comparison of algorithms for incoming atmospheric long-wave radiation, *Water Resour. Res.*, 45(3), <https://doi.org/10.1029/2008wr007394>.

Freitag, H. P. (1994), Calibration procedures and instrumental accuracy estimates of TAO temperature, relative humidity and radiation measurements.

Freitag, H. P. (1999), COARE seacat data : Calibrations and quality control procedures, Producer.

Freitag, H. P. (2001), Calibration procedures and instrumental accuracies for ATLAS wind measurements, Producer.

Frouin, R., C. Gautier, & J. J. Morcrette (1988), Downward longwave irradiance at the ocean surface from satellite data: Methodology and in situ validation, *J Geophys Res-Oceans*, 93(C1), 597-619, <https://doi.org/10.1029/JC093iC01p00597>.

Fung, I. Y., D. E. Harrison, & A. A. Lacis (1984), On the variability of the net longwave radiation at the ocean surface, *Rev Geophys*, 22(2), 177-193, <https://doi.org/10.1029/RG022i002p00177>.

Gelaro, R., W. McCarty, M. J. Suárez, R. Todling, A. Molod, L. Takacs, et al. (2017), The modern-era retrospective analysis for research and applications, version 2 (MERRA-2), *J. Climate*, 30(14), 5419-5454, <https://doi.org/10.1175/Jcli-D-16-0758.1>.

Grayek, S., J. Staneva, J. Schulz-Stellenfleth, W. Petersen, & E. V. Stanev (2011), Use of FerryBox surface temperature and salinity measurements to improve model based state estimates for the German Bight, *J Marine Syst.*, 88(1), 45-59, <https://doi.org/10.1016/j.jmarsys.2011.02.020>.

Gubler, S., S. Gruber, & R. S. Purves (2012), Uncertainties of parameterized surface downward clear-sky shortwave and all-sky longwave radiation, *Atmos. Chem. Phys.*, 12(11), 5077-5098, <https://doi.org/10.5194/acp-12-5077-2012>.

Guo, Y., J. Cheng, & S. Liang (2019), Comprehensive assessment of parameterization methods for estimating clear-sky surface downward longwave radiation, *Theoretical and Applied Climatology*, 135(3), 1045-1058, <https://doi.org/10.1007/s00704-018-2423-7>.

Habets, F., J. Noilhan, C. Golaz, J. P. Goutorbe, P. Lacarrère, E. Leblois, et al. (1999), The ISBA surface scheme in a macroscale hydrological model applied to the Hapex-Mobilhy area: Part I: Model and database, *Journal of Hydrology*, 217(1), 75-96, [https://doi.org/10.1016/S0022-1694\(99\)00019-0](https://doi.org/10.1016/S0022-1694(99)00019-0).

Hack, J. J. (1998), Sensitivity of the simulated climate to a diagnostic formulation for cloud liquid water, *J. Climate*, 11(7), 1497-1515, [https://doi.org/10.1175/1520-0442\(1998\)011<1497:SOTSCT>2.0.CO;2](https://doi.org/10.1175/1520-0442(1998)011<1497:SOTSCT>2.0.CO;2).

Henderson - Sellers, B. (1984), A new formula for latent heat of vaporization of water as a function of temperature, *Quart J Roy Meteor Soc.*, 110(466), 1186-1190, <https://doi.org/10.1002/QJ.49711046626>.

Hersbach, H., B. Bell, P. Berrisford, S. Hirahara, A. Horányi, J. Muñoz - Sabater, et al. (2020), The ERA5 global reanalysis, *Quart J Roy Meteor Soc.*, 146(730), 1999-2049, <https://doi.org/10.1002/qj.3803>.

Hoffmann, L., G. Günther, D. Li, O. Stein, X. Wu, S. Griessbach, et al. (2019), From ERA-Interim to ERA5: the considerable impact of ECMWF's next-generation reanalysis on Lagrangian transport simulations, *Atmos. Chem. Phys.*, 19(5), 3097-3124, <https://doi.org/10.5194/acp-19-3097-2019>.

Idso, S. B., & R. D. Jackson (1969), Thermal radiation from the atmosphere, *J. Geophys. Res.*, 74(23), 5397-5403, <https://doi.org/10.1029/JC074i023p05397>.

Iziomon, M. G., H. Mayer, & A. Matzarakis (2003), Downward atmospheric longwave irradiance under clear and cloudy skies: Measurement and parameterization, *J Atmos Sol-Terr Phy*, 65(10), 1107-1116, <https://doi.org/doi:10.1016/j.jastp.2003.07.007>.

916 Jiang, B., S. Liang, H. Ma, X. Zhang, Z. Xiao, X. Zhao, et al. (2016), GLASS daytime all-wave net radiation
917 product: Algorithm development and preliminary validation, *Remote Sens-Basel*, 8(3),
918 <https://doi.org/10.3390/rs8030222>.

919 Jiang, B., Y. Zhang, S. Liang, G. Wohlfahrt, A. Arain, A. Cescatti, et al. (2015), Empirical estimation of daytime net
920 radiation from shortwave radiation and ancillary information, *Agr Forest Meteor.*, 211-212, 23-36,
921 <https://doi.org/10.1016/j.agrformet.2015.05.003>.

922 Josey, S. A. (2003), A new formula for determining the atmospheric longwave flux at the ocean surface at mid-high
923 latitudes, *J Geophys Res-Oceans*, 108(C4), <https://doi.org/10.1029/2002jc001418>.

924 Josey, S. A., D. Oakley, & R. W. Pascal (1997), On estimating the atmospheric longwave flux at the ocean surface
925 from ship meteorological reports, *J Geophys Res-Oceans*, 102(C13), 27961-27972,
926 <https://doi.org/10.1029/97jc02420>.

927 Jost, G., R. Dan Moore, M. Weiler, D. R. Gluns, & Y. Alila (2009), Use of distributed snow measurements to test
928 and improve a snowmelt model for predicting the effect of forest clear-cutting, *Journal of Hydrology*, 376(1), 94-
929 106, <https://doi.org/10.1016/j.jhydrol.2009.07.017>.

930 Kjaersgaard, J. H., F. L. Plauborg, & S. Hansen (2007), Comparison of models for calculating daytime long-wave
931 irradiance using long term data set, *Agr Forest Meteor.*, 143(1-2), 49-63,
932 <https://doi.org/10.1016/j.agrformet.2006.11.007>.

933 Lake, B. J. (2003), Calibration procedures and instrumental accuracy estimates of ATLAS air temperature and
934 relative humidity measurements, NOAA Tech. Memo. OAR PMEL-123, 23.

935 Li, M., & C. F. M. Coimbra (2019), On the effective spectral emissivity of clear skies and the radiative cooling
936 potential of selectively designed materials, *Int J Heat Mass Tran*, 135, 1053-1062,
937 <https://doi.org/https://doi.org/10.1016/j.ijheatmasstransfer.2019.02.040>.

938 Li, M., Y. Jiang, & C. F. M. Coimbra (2017), On the determination of atmospheric longwave irradiance under all-
939 sky conditions, *Solar Energy*, 144, 40-48, <https://doi.org/https://doi.org/10.1016/j.solener.2017.01.006>.

940 Lindau, R. (2012), *Climate atlas of the Atlantic Ocean: derived from the comprehensive ocean atmosphere data set*
941 *(COADS)*, Springer Science & Business Media.

942 Lohmann, D., E. Raschke, B. Nijssen, & D. P. Lettenmaier (1998), Regional scale hydrology: II. Application of the
943 VIC-2L model to the Weser River, Germany, *Hydrological sciences journal*, 43(1), 143-158,
944 <https://doi.org/10.1080/02626669809492108>.

945 McPhaden, M. J., K. Ando, B. Bourles, H. P. Freitag, R. Lumpkin, Y. Masumoto, et al. (2010), The global tropical
946 moored buoy array, *Proceedings of OceanObs*, 9, 668-682.

947 McPhaden, M. J., A. J. Busalacchi, R. Cheney, J. R. Donguy, K. S. Gage, D. Halpern, et al. (1998), The Tropical
948 Ocean-Global Atmosphere observing system: A decade of progress, *J Geophys Res-Oceans*, 103(C7), 14169-14240,
949 <https://doi.org/10.1029/97JC02906>.

950 McPhaden, M. J., G. Meyers, K. Ando, Y. Masumoto, V. S. N. Murty, M. Ravichandran, et al. (2009), RAMA: the
951 research moored array for African-Asian-Australian monsoon analysis and prediction, *Bull. Amer. Meteor. Soc.*,
952 90(4), 459-480, <https://doi.org/10.1175/2008bams2608.1>.

953 Medovaya, M., D. E. Waliser, R. A. Weller, & M. J. McPhaden (2002), Assessing ocean buoy shortwave
954 observations using clear-sky model calculations, *J Geophys Res-Oceans*, 107,
955 <https://doi.org/10.1029/2000JC000558>.

956 Meyers, T. P., & R. F. Dale (1983), PREDICTING DAILY INSOLATION WITH HOURLY CLOUD HEIGHT
957 AND COVERAGE, *J Clim Appl Meteorol*, 22(4), 537-545, [https://doi.org/10.1175/1520-0450\(1983\)022<0537:pdiwhc>2.0.co;2](https://doi.org/10.1175/1520-0450(1983)022<0537:pdiwhc>2.0.co;2).

958 Mills, G. (1997), An urban canopy-layer climate model, *Theoretical and applied climatology*, 57(3), 229-244,
959 <https://doi.org/10.1007/BF00863615>.

960 Mousavi Maleki, S., H. Hizam, & C. Gomes (2017), Estimation of Hourly, Daily and Monthly Global Solar
961 Radiation on Inclined Surfaces: Models Re-Visited, *Energies*, 10(1), <https://doi.org/10.3390/en10010134>.

962 Moyer, K. A., & R. A. Weller (1997), Observations of surface forcing from the Subduction Experiment: A
963 comparison with global model products and climatological datasets, *J. Climate*, 10(11), 2725-2742,
964 [https://doi.org/10.1175/1520-0442\(1997\)010<2725:OOSFFT>2.0.CO;2](https://doi.org/10.1175/1520-0442(1997)010<2725:OOSFFT>2.0.CO;2).

965 Nandan, R., M. V. Ratnam, V. R. Kiran, & D. N. Naik (2022), Retrieval of cloud liquid water path using radiosonde
966 measurements: Comparison with MODIS and ERA5, *J Atmos Sol-Terr Phy*, 227,
967 <https://doi.org/10.1016/j.jastp.2021.105799>.

968 Nice, K. A., A. M. Coutts, & N. J. Tapper (2018), Development of the VTUF-3D v1.0 urban micro-climate model to
969 support assessment of urban vegetation influences on human thermal comfort, *Urban Climate*, 24, 1052-1076,
970 <https://doi.org/10.1016/j.uclim.2017.12.008>.

972 Ogunjobi, K. O., & Y. J. Kim (2004), Ultraviolet (0.280–0.400 μm) and broadband solar hourly radiation at
 973 Kwangju, South Korea: analysis of their correlation with aerosol optical depth and clearness index, *Atmos Res*,
 974 71(3), 193-214, <https://doi.org/10.1016/j.atmosres.2004.05.001>.
 975 Oleson, K. W., G. B. Bonan, J. Feddema, M. Vertenstein, & C. S. B. Grimmond (2008), An Urban Parameterization
 976 for a Global Climate Model. Part I: Formulation and Evaluation for Two Cities, *J. Appl. Meteor. Climatol.*, 47(4),
 977 1038-1060, <https://doi.org/10.1175/2007JAMC1597.1>.
 978 Pascal, R. W., & S. A. Josey (2000), Accurate Radiometric Measurement of the Atmospheric Longwave Flux at the
 979 Sea Surface, *J. Atmos. Oceanic Technol.*, 17(9), 1271-1282, [https://doi.org/10.1175/1520-0426\(2000\)017<1271:ARMOTA>2.0.CO;2](https://doi.org/10.1175/1520-0426(2000)017<1271:ARMOTA>2.0.CO;2).
 980 Paul, B. (2021), Retrospective on the resource for radiative cooling, *Journal of Photonics for Energy*, 11(4), 042106,
 981 <https://doi.org/10.1117/1.JPE.11.042106>.
 982 Pauwels, V. R. N., N. E. C. Verhoest, G. J. M. De Lannoy, V. Guissard, C. Lucau, & P. Defourny (2007),
 983 Optimization of a coupled hydrology–crop growth model through the assimilation of observed soil moisture and leaf
 984 area index values using an ensemble Kalman filter, *Water Resour Res*, 43(4),
 985 <https://doi.org/10.1029/2006WR004942>.
 986 Payne, R. E. (1972), Albedo of the sea surface, *J Atmos Sci*, 29(5), 959-970, [https://doi.org/10.1175/1520-0469\(1972\)029<0959:AOTSS>2.0.CO;2](https://doi.org/10.1175/1520-0469(1972)029<0959:AOTSS>2.0.CO;2).
 987 Payne, R. E., & S. P. Anderson (1999), A new look at calibration and use of Eppley precision infrared radiometers.
 988 Part II: Calibration and use of the Woods Hole Oceanographic Institution improved meteorology precision infrared
 989 radiometer, *J. Atmos. Oceanic Technol.*, 16(6), 739-751, [https://doi.org/10.1175/1520-0426\(1999\)016<0739:ANLACA>2.0.CO;2](https://doi.org/10.1175/1520-0426(1999)016<0739:ANLACA>2.0.CO;2).
 990 Pinardi, N., I. Allen, E. Demirov, P. De Mey, G. Korres, A. Lascaratos, et al. (2003), The Mediterranean ocean
 991 forecasting system: first phase of implementation (1998–2001), *Annales Geophysicae*, 21(1), 3-20,
 992 <https://doi.org/10.5194/angeo-21-3-2003>.
 993 Pinker, R. T., A. Bentamy, K. B. Katsaros, Y. Ma, & C. Li (2014), Estimates of net heat fluxes over the Atlantic
 994 Ocean, *J Geophys Res-Oceans*, 119(1), 410-427, <https://doi.org/10.1002/2013JC009386>.
 995 Pinker, R. T., B. Zhang, R. A. Weller, & W. Chen (2018), Evaluating Surface Radiation Fluxes Observed From
 996 Satellites in the Southeastern Pacific Ocean, *Geophys Res Lett*, 45(5), 2404-2412,
 997 <https://doi.org/10.1002/2017gl076805>.
 1000 Prata, A. (1996), A new longwave formula for estimating downward clear - sky radiation at the surface, *Quart J Roy Meteor Soc*, 122(533), 1127-1151, <https://doi.org/10.1002/qj.49712253306Citations>: 348.
 1001 Rigon, R., G. Bertoldi, & T. M. Over (2006), GEOTop: A distributed hydrological model with coupled water and
 1002 energy budgets, *Journal of Hydrometeorology*, 7(3), 371-388, <https://doi.org/10.1175/JHM497.1>.
 1003 Robinson, G. D. (1947), Notes on the measurement and estimation of atmospheric radiation, *Quart J Roy Meteor Soc*, 73(315 - 316), 127-150, <https://doi.org/10.1002/qj.49707331510>.
 1004 Robinson, G. D. (1950), Notes on the measurement and estimation of atmospheric radiation–2, *Quart J Roy Meteor Soc*, 76(327), 37-51, <https://doi.org/10.1002/qj.49707632705>.
 1005 Rossow, W. B., & Y. C. Zhang (1995), Calculation of surface and top of atmosphere radiative fluxes from physical
 1006 quantities based on ISCCP data sets: 2. Validation and first results, *J Geophys Res-Atmos*, 100(D1), 1167-1197,
 1007 <https://doi.org/10.1029/94JD02746>.
 1008 Rutan, D. A., S. Kato, D. R. Doelling, F. G. Rose, L. T. Nguyen, T. E. Caldwell, & N. G. Loeb (2015), CERES
 1009 synoptic product: Methodology and validation of surface radiant flux, *J. Atmos. Oceanic Technol.*, 32(6), 1121 -
 1010 1143, <https://doi.org/10.1175/JTECH-D-14-00165.1>.
 1011 Saltelli, A., S. Tarantola, & K.-S. Chan (1999), A quantitative model-independent method for global sensitivity
 1012 analysis of model output, *Technometrics*, 41(1), 39-56, <https://doi.org/10.2307/1270993>.
 1013 Satterlund, D. R. (1979), IMPROVED EQUATION FOR ESTIMATING LONG-WAVE-RADIATION FROM
 1014 THE ATMOSPHERE, *Water Resour Res*, 15(6), 1649-1650, <https://doi.org/10.1029/WR015i006p01649>.
 1015 Saucier, F. J., F. Roy, D. Gilbert, P. Pellerin, & H. Ritchie (2003), Modeling the formation and circulation processes
 1016 of water masses and sea ice in the Gulf of St. Lawrence, Canada, *J Geophys Res-Oceans*, 108(C8),
 1017 <https://doi.org/10.1029/2000JC000686>.
 1018 Schlosser, C. A., A. Robock, K. Y. Vinnikov, N. A. Speranskaya, & Y. Xue (1997), 18-Year Land-Surface
 1019 Hydrology Model Simulations for a Midlatitude Grassland Catchment in Valdai, Russia, *Mon. Wea. Rev.*, 125(12),
 1020 3279-3296, [https://doi.org/10.1175/1520-0493\(1997\)125<3279:YLSHMS>2.0.CO;2](https://doi.org/10.1175/1520-0493(1997)125<3279:YLSHMS>2.0.CO;2).
 1021 Schulz, E. W., S. A. Josey, & R. Verein (2012), First air-sea flux mooring measurements in the Southern Ocean,
 1022 *Geophys Res Lett*, 39(16), n/a-n/a, <https://doi.org/10.1029/2012gl052290>.
 1023
 1024
 1025
 1026

Field Code Changed

1027 Schwarzschild, K. (1914), *Ueber Diffusion und Absorption in der Sonnenatmosphäre*. Sridhar, V., & R. L. Elliott
 1028 (2002), On the development of a simple downwelling longwave radiation scheme, *Agr Forest Meteor.*, 112(3), 237-
 1029 243, [https://doi.org/10.1016/S0168-1923\(02\)00129-6](https://doi.org/10.1016/S0168-1923(02)00129-6).
 1030 Staley, D. O., & G. M. Jurica (1972), Effective Atmospheric Emissivity under Clear Skies, *J Appl Meteorol*, 11(2),
 1031 349-356, [https://doi.org/10.1175/1520-0450\(1972\)011<0349:EAEUCS>2.0.CO;2](https://doi.org/10.1175/1520-0450(1972)011<0349:EAEUCS>2.0.CO;2).
 1032 Swinbank, W. C. (1963), Long - wave radiation from clear skies, *Quart J Roy Meteor Soc*, 89(381), 339-348,
 1033 <https://doi.org/10.1002/qj.49708938105>.
 1034 Thandlam, V., & H. Rahaman (2019), Evaluation of surface shortwave and longwave downwelling radiations over
 1035 the global tropical oceans, *SN Applied Sciences*, 1(10), <https://doi.org/10.1007/s42452-019-1172-2>.
 1036 Tiedtke, M. (1993), Representation of Clouds in Large-Scale Models, *Mon. Wea. Rev.*, 121(11), 3040-3061,
 1037 [https://doi.org/10.1175/1520-0493\(1993\)121<3040:ROCILS>2.0.CO;2](https://doi.org/10.1175/1520-0493(1993)121<3040:ROCILS>2.0.CO;2).
 1038 Vanhellemont, Q. (2020), Automated water surface temperature retrieval from Landsat 8/TIRS, *Remote Sens*
 1039 *Environ*, 237, <https://doi.org/10.1016/j.rse.2019.111518>.
 1040 Vertessy, R. A., T. J. Hatton, P. J. O'Shaughnessy, & M. D. A. Jayasuriya (1993), Predicting water yield from a
 1041 mountain ash forest catchment using a terrain analysis based catchment model, *Journal of Hydrology*, 150(2), 665-
 1042 700, [https://doi.org/10.1016/0022-1694\(93\)90131-R](https://doi.org/10.1016/0022-1694(93)90131-R).
 1043 Viúdez-Mora, A., M. Costa-Surós, J. Calbó, & J. A. González (2015), Modeling atmospheric longwave radiation at
 1044 the surface during overcast skies: The role of cloud base height, *J Geophys Res-Atmos*, 120(1), 199-214,
 1045 <https://doi.org/10.1002/2014jd022310>.
 1046 Wang, K., & S. Liang (2009a), Global atmospheric downward longwave radiation over land surface under all-sky
 1047 conditions from 1973 to 2008, *J Geophys Res-Atmos*, 114(D19),
 1048 <https://doi.org/https://doi.org/10.1029/2009JD011800>.
 1049 Wang, T., J. Shi, Y. Ma, H. Letu, & X. Li (2020), All-sky longwave downward radiation from satellite
 1050 measurements: General parameterizations based on LST, column water vapor and cloud top temperature, *ISPRS*
 1051 *Journal of Photogrammetry and Remote Sensing*, 161, 52-60, <https://doi.org/10.1016/j.isprsjprs.2020.01.011>.
 1052 Wang, W., & S. Liang (2009b), Estimation of high-spatial resolution clear-sky longwave downward and net
 1053 radiation over land surfaces from MODIS data, *Remote Sens Environ*, 113(4), 745-754,
 1054 <https://doi.org/10.1016/j.rse.2008.12.004>.
 1055 Yang, F., & J. Cheng (2020), A framework for estimating cloudy sky surface downward longwave radiation from
 1056 the derived active and passive cloud property parameters, *Remote Sens Environ*, 248,
 1057 <https://doi.org/10.1016/j.rse.2020.111972>.
 1058 Young, A. H., K. R. Knapp, A. Inamdar, W. Hankins, & W. B. Rossow (2018), The international satellite cloud
 1059 climatology project H-Series climate data record product, *Earth System Science Data*, 10(1), 583-593,
 1060 <https://doi.org/10.5194/essd-10-583-2018>.
 1061 Yu, S., X. Xin, Q. Liu, H. Zhang, & L. Li (2018), Comparison of Cloudy-Sky Downward Longwave Radiation
 1062 Algorithms Using Synthetic Data, Ground-Based Data, and Satellite Data, *J Geophys Res-Atmos*, 123(10), 5397-
 1063 5415, <https://doi.org/10.1029/2017jd028234>.
 1064 Zapadka, T., S. B. Woźniak, & B. Woźniak (2001), A simple formula for the net long-wave radiation flux in the
 1065 Southern Baltic Sea, *Oceanologia*, 43(3), 265-277.
 1066 Zhou, Y., & R. D. Cess (2001), Algorithm development strategies for retrieving the downwelling longwave flux at
 1067 the Earth's surface, *J Geophys Res-Atmos*, 106(D12), 12477-12488, <https://doi.org/10.1029/2001jd900144>.
 1068 Zhou, Y., D. P. Kratz, A. C. Wilber, S. K. Gupta, & R. D. Cess (2007), An improved algorithm for retrieving
 1069 surface downwelling longwave radiation from satellite measurements, *J Geophys Res-Atmos*, 112(D15),
 1070 <https://doi.org/10.1029/2006jd008159>.
 1071